

Sites NGHP-01-20

By T. Collett, M. Riedel, J. Cochran, R. Boswell, J. Presley, P. Kumar, A. Sathe,
A. Sethi, M. Lall, and the National Gas Hydrate Program Expedition 01 Scientists

Scientific Investigations Report 2012–5054

U.S. Department of the Interior
U.S. Geological Survey

Contents

Background and Objectives.....	1219
Operations.....	1219
Hole NGHP-01-20A.....	1219
Hole NGHP-01-20B.....	1222
Lithostratigraphy.....	1223
Lithostratigraphic Units.....	1223
Lithostratigraphic unit I.....	1223
Gas Hydrate Occurrence.....	1227
Inorganic Geochemistry.....	1233
Interstitial Water Chloride and Salinity.....	1233
Sulfate and Alkalinity Concentrations: Characterization of the SMI.....	1234
Bromide Concentrations.....	1235
Organic Geochemistry.....	1235
Microbiology.....	1241
Hole NGHP-01-20A.....	1241
Hole NGHP-01-20B.....	1241
Physical Properties.....	1248
Infrared Imaging.....	1248
Environmental Conditions.....	1248
Infrared Images.....	1248
Core-End-Temperature Readings.....	1253
Index Properties.....	1253
Strength.....	1253
Electrical Resistivity.....	1258
P-Wave Velocity.....	1258
Magnetic Susceptibility.....	1258
Thermal Conductivity.....	1263
Downhole Temperature Measurements.....	1263
Pressure Coring.....	1263
Downhole Logging.....	1263
References Cited.....	1264

Figures

1. Bathymetric map of the Krishna-Godavari Basin with Site NGHP-01-20.....	1220
2. Seismic line AD-94-11 crossing Site NGHP-01-20.....	1221
3. Map showing all holes occupied at Site NGHP-01-20.....	1222
4. Lithostratigraphic summary of Holes NGHP-01-20A and NGHP-01-20B.....	1224
5. Sand and silt laminae and beds.....	1225
6. A, Visible foraminifera; and B and C, shell fragments observed throughout Unit I.....	1228
7. Authigenic carbonate occurrences in Unit I.....	1229

8.	A, Summary of the major lithologic components in smear slides and coarse fraction data plotted from percent visual estimation. B, Major lithologic components in coarse fraction and smear slide; shown for clarity as individual abundance plots. C, Grain size distribution determined from smear slide sand, silt, and clay percentage estimations	1230
9.	Concentration-depth profiles of A, chloride and B, salinity at Hole NGHP-01-20A. C, Cross plot between dissolved chloride concentration and salinity, showing a good correspondence for samples deeper than 40 mbsf, where both parameters are primarily influenced by dilution of the fluids by hydrate dissociation	1239
10.	A, Concentration-depth profiles of alkalinity; B, sulfate; and C, sulfate, methane, and alkalinity at Hole NGHP-01-20A	1240
11.	Concentration-depth profile of dissolved bromide at Hole NGHP-01-20A	1241
12.	Plot of headspace methane gas concentration with depth for Hole NGHP-01-20A	1244
13.	Plot of headspace carbon dioxide gas concentration with depth for Hole NGHP-01-20A	1245
14.	Plot of methane to carbon dioxide gas ratio with depth for headspace, void gas, and PCS gas for Hole NGHP-01-20A	1246
15.	Catwalk temperature and humidity measurements as a function of time during drilling operations at Site NGHP-01-20	1249
16.	Infrared imaging and the derived downhole temperature profile for Site NGHP-01-20	1251
17.	Comparison of core-end infrared images and cross-core temperature profiles from two different parts of Hole NGHP-01-20A: Cores NGHP-01-20A-10X and NGHP-01-20A-16X	1252
18.	Profiles of core recovery, index, and strength properties for Site NGHP-01-20	1256
19.	Profiles of infrared images, core recovery, electrical resistivity, acoustic <i>P</i> -wave velocity, magnetic susceptibility, and thermal conductivity for Site NGHP-01-20	1257
20.	Shear strengths normalized to the effective vertical stress versus sub-bottom depth for Hole NGHP-01-20A	1260
21.	Peak and remolded vane shear strengths and sensitivity for Hole NGHP-01-20A	1260
22.	Apparent formation factor versus sub-bottom depth for Hole NGHP-01-20A	1263
23.	Geothermal gradient and estimated depth to the BSR from <i>in situ</i> temperature measurements for Hole NGHP-01-20A	1264

Tables

1.	Smear-slide data for Holes NGHP-01-20A and NGHP-01-20B	1226
2.	Coarse fraction (>63 μm) sieve data for Holes NGHP-01-20A and NGHP-01-20B	1234
3.	Silt laminae and beds for Site NGHP-01-20	1236
4.	Interstitial-water data for Hole NGHP-01-20A	1237
5.	Interstitial-water data corrected for drill-water contamination based on sulfate concentration, for Hole NGHP-01-20A	1238
6.	Headspace gas composition for Site NGHP-01-20	1242
7.	List of microbiological samples taken for Site NGHP-01-20	1247

8.	List of infrared images collected from Hole NGHP-01-20A	1250
9.	List of infrared image files collected from section ends from Hole NGHP-01-20A.....	1250
10.	List of temperature probe data collected at bottom of cores from Hole NGHP-01-20A	1253
11.	Moisture and density physical properties for Hole NGHP-01-20A.....	1254
12.	Vane shear strength results for Hole NGHP-01-20A.....	1258
13.	Pocket Penetrometer strength results for Hole NGHP-01-20A.....	1259
14.	Wenner array electrical resistivity and formation factor results for Hole NGHP-01-20A.....	1261
15.	Contact <i>P</i> -Wave velocity results determined on split cores sections from Hole NGHP-01-20A	1263
16.	Thermal conductivity results for Hole NGHP-01-20A	1263
17.	<i>In situ</i> temperature estimates for Hole NGHP-01-20A.....	1264

Site NGHP-01-20

By T. Collett, M. Riedel, J. Cochran, R. Boswell, J. Presley, P. Kumar, A. Sathe, A. Sethi, M. Lall, and the National Gas Hydrate Program Expedition 01 Scientists

Background and Objectives

Site NGHP-01-20 (Prospectus Site KGGH05) is located at long 15°48.5671'N, lat 81°50.5760'E in the Krishna-Godavari Basin (figs. 1 and 2). The water depth is ~1,146 m. This site was targeted as an add-on site after the main expedition was completed and Site NGHP-01-17 in the Andaman Islands and Sites NGHP-01-18 and NGHP-01-19 in the Mahanadi Basin were drilled.

The objectives of the work carried out at this site follow the general objectives of the India NGHP Expedition 01:

- Determine if gas hydrate is indeed present at this site and if the seismic reflection is a gas hydrate-related BSR;
- Study the occurrence of gas hydrate and establish the background geochemical, geological, geophysical, and microbiological baselines for gas hydrate proxy-studies;
- Define the relationship between the sedimentology and structure of the sediments and the occurrence and concentration of gas hydrate;
- Calibrate remote sensing data such as seismic data by acquiring wire-line log data;
- Assess the controls on the occurrence of gas hydrate in a highly deformed geologic setting.

Site NGHP-01-20 is located on a small structural high ~100 min TWT (~75 m) above the adjacent seafloor. Seismic line AD-94-11 crossing Site NGHP-01-20 shows a strong BSR event at the drill site at an estimated depth of 220 mbsf. However, this BSR is not laterally extensive and is restricted to a few hundred meters around the drill site. Further to the SE along the seismic line, the BSR reappears for about another 1,000 m (until trace 95), but the reflection strength is strongly reduced. Towards the NW, a strong amplitude band at a depth of ~260–280 min TWT below seafloor can be seen. This reflection band is not parallel to the seafloor and exhibits a complex reflection pattern such that no single reflection phase can be isolated. It is therefore difficult to determine if this reflection band is a BSR. However, the increase in reflection amplitude may be the effect of free gas trapped below the gas hydrate stability zone.

Operations

This operations summary covers the Leg 4 transit from Site NGHP-01-19 (MNGH-Gap Site) to Site NGHP-01-18 (MNGH-Reliance 5), the beacon recovery at Site NGHP-01-18, the transit to Site NGHP-01-20 (KGGH05), and drilling/coring operations for Holes NGHP-01-20A and NGHP-01-20B (fig. 3). Schedule details and statistics for this site can be found as Appendixes:

- Appendix 1: NGHP Expedition 01 Operations Schedules
- Appendix 2: NGHP Expedition 01 Operations Statistics

Included in the Methods chapter and the glossary is a list of standard or commonly used operations terms and acronyms.

Hole NGHP-01-20A

Hole NGHP-01-20A was occupied on Leg 4 of NGHP Expedition 01. This was the first of two holes drilled at alternate Site NGHP-01-20 (KGGH05).

After departing Site NGHP-01-19 (MNGH-Gap Site), the vessel transited north to the previously occupied Site NGHP-01-18 (MNGH-Reliance 5) to recover the positioning beacon left at that site earlier. Beacon recovery at this site was not initially attempted because the rough sea state and strong current conditions prevalent at the time significantly increased the potential of beacon loss. The 12.0 NMI transit to Site NGHP-01-18 was completed in 1.75 hr at an average speed of 7.5 knots. Subsequent lowering of thrusters/hydrophones, release and recovery of the beacon, and raising of the thrusters/hydrophones required another 1.25 hr. The vessel was switched to cruise mode and was underway for Site NGHP-01-20 at 0700 hr on 9 August.

The 301 NMI transit from Site NGHP-01-18 to Site NGHP-01-20 was completed in 31.9 hr at an average speed of 9.4 knots. The vessel was switched from cruise mode to DP control at 1442 hr on 10 August, thrusters were lowered, and a positioning beacon was deployed on the prospectus coordinates at 1522 hr. The ice bath was installed in the moon pool and the same BHA as was used on the previous site was deployed from its racked position in the derrick.

Hole NGHP-01-20A was planned as a continuous APC/XCB cored hole to 300.0 mbsf with two packages of pressure cores targeting the gas hydrate stability zone. Temperature

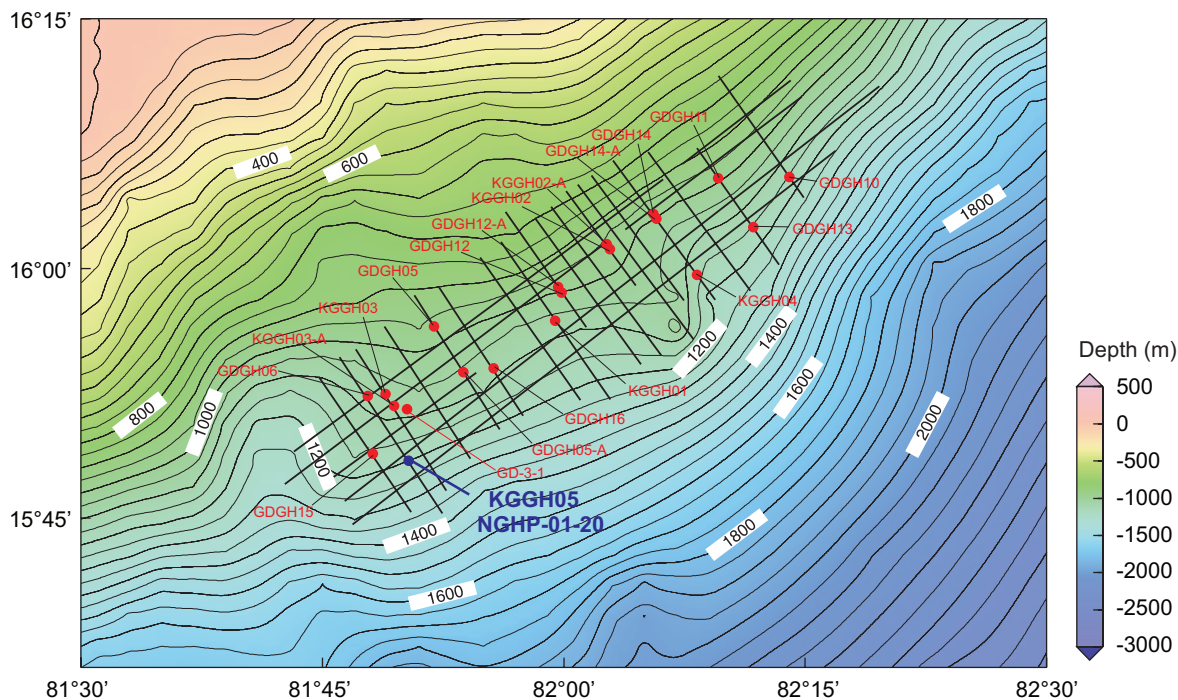


Figure 1. Bathymetric map of the Krishna-Godavari Basin with Site NGHP-01-20 (Prospectus Site KGGH-05).

measurements were also to be taken using the APCT-3 and DVTP systems to define a thermal gradient from seafloor to total depth. The hole was to culminate with two suites of wire-line logs using the triple combo and FMS-sonic tool strings. There was no VSP logging planned. Ultimately, two holes were drilled/cored in an unsuccessful attempt to overcome hole stability problems that precluded much of the pressure coring and logging program planned for the site.

The drill string was tripped to bottom. The bit was positioned at a depth of 1,146.0 mbrf and the first attempt was made to spud Hole NGHP-01-20A. This core barrel recovered only water so the drill string was lowered an additional 5.0 m to 1,151.0 mbrf. This core barrel recovered <2.0 m of core and this was judged inadequate by the science contingent. The bit was lowered a third time, this time by 3.0 m, to 1,154.0 mbrf. Hole NGHP-01-20A was subsequently spudded at 1950 hr on 10 August establishing a seafloor depth of 1,157.9 mbrf. The PDR depth for this site, corrected to the rig floor DES, was 1,157.4 mbrf. Core NGHP-01-20A-01H was on-deck at 2000 hr. APC Coring (APC) continued only through Core NGHP-01-20A-03H to a depth of 22.9 mbsf, where refusal was reached with a 7.8 m advance.

A single temperature measurement was taken using the APCT-3 shoe on Core NGHP-01-20A-03H at a depth of 22.9 mbsf.

Coring continued with the XCB coring system recovering Cores NGHP-01-20A-04X through NGHP-01-20A-08X to a depth of 70.9 mbsf. A single DVTP temperature measurement was successfully taken at that depth. This was followed by XCB Cores NGHP-01-20A-09X through NGHP-01-20A-13X to a depth of 102.8 mbsf. Core recovery and quality was poor

on these initial XCB cores and included significant reduction in core diameter, which led to several changes to the coring operation. First, the reduction in core diameter was attributed to possible malfunctioning of the 4-petal or 9-finger core catchers. To combat this, the standard springs in the 4-petal core catcher were replaced with smaller/weaker springs. In addition, several short or XCB “half” cores (Core NGHP-01-20A-11X through NGHP-01-20A-13X; 90.2 mbsf to 102.8 mbsf) were cut in an attempt to increase core recovery. This was moderately successful; however, the core damage problem persisted. Coring was suspended after Core NGHP-01-20A-13X at 102.8 mbsf because of hole stability issues that may have been the main cause of the core recovery and quality problems. The hole annulus appeared to be packing off with cuttings or hole sloughing which led to significant fill on-bottom between connections and also resulted in a pump-off effect at the bit. This meant that the driller was unable to maintain sufficient WOB to conduct optimum coring operations. The packing off manifested itself as higher pump pressures and higher than normal rotating torque. The size and frequency of mud sweeps had no effect on the problem. Therefore, at 1000 hr on 11 August, coring was suspended and 2.5 hr were used for some badly needed hole conditioning. A wiper trip was conducted to 35.1 mbsf and back to TD with Sepiolite mud sweeps pumped before and after the wiper trip.

At 1230 hr, coring resumed with the recovery of XCB Cores NGHP-01-20A-14X through NGHP-01-20A-19X to a depth of 147.8 mbrf. XCB half cores were cut with Cores NGHP-01-20A-14X and NGHP-01-20A-15X. However, except for one excellent core, the problems persisted both with the hole condition and the coring program.

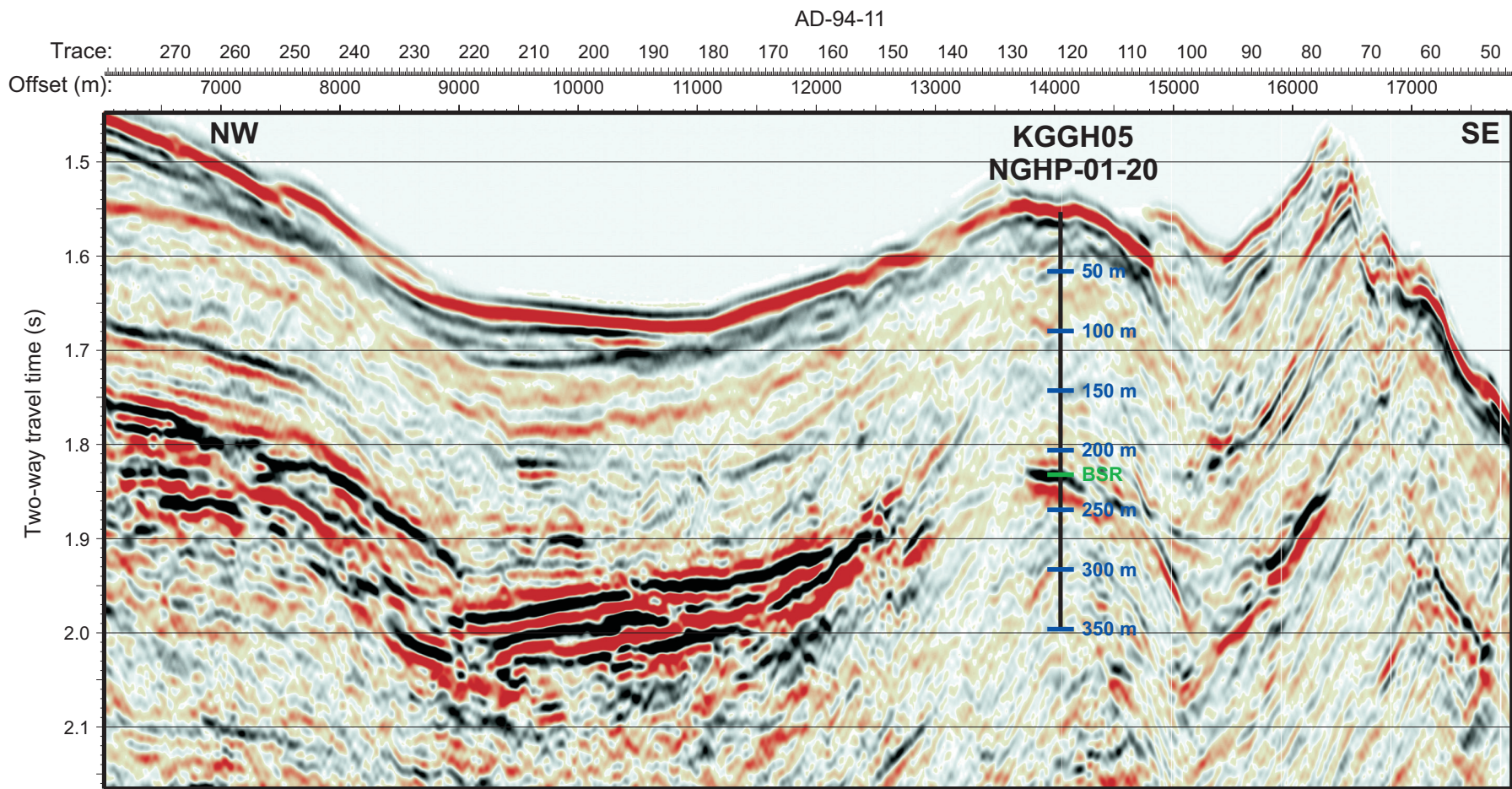


Figure 2. Seismic line AD-94-11 (NW-SE oriented) crossing Site NGHP-01-20. The site is located at around trace 122. Depth of formation tops were estimated using a constant velocity of 1,580 m/s. [m/s, meters per second]

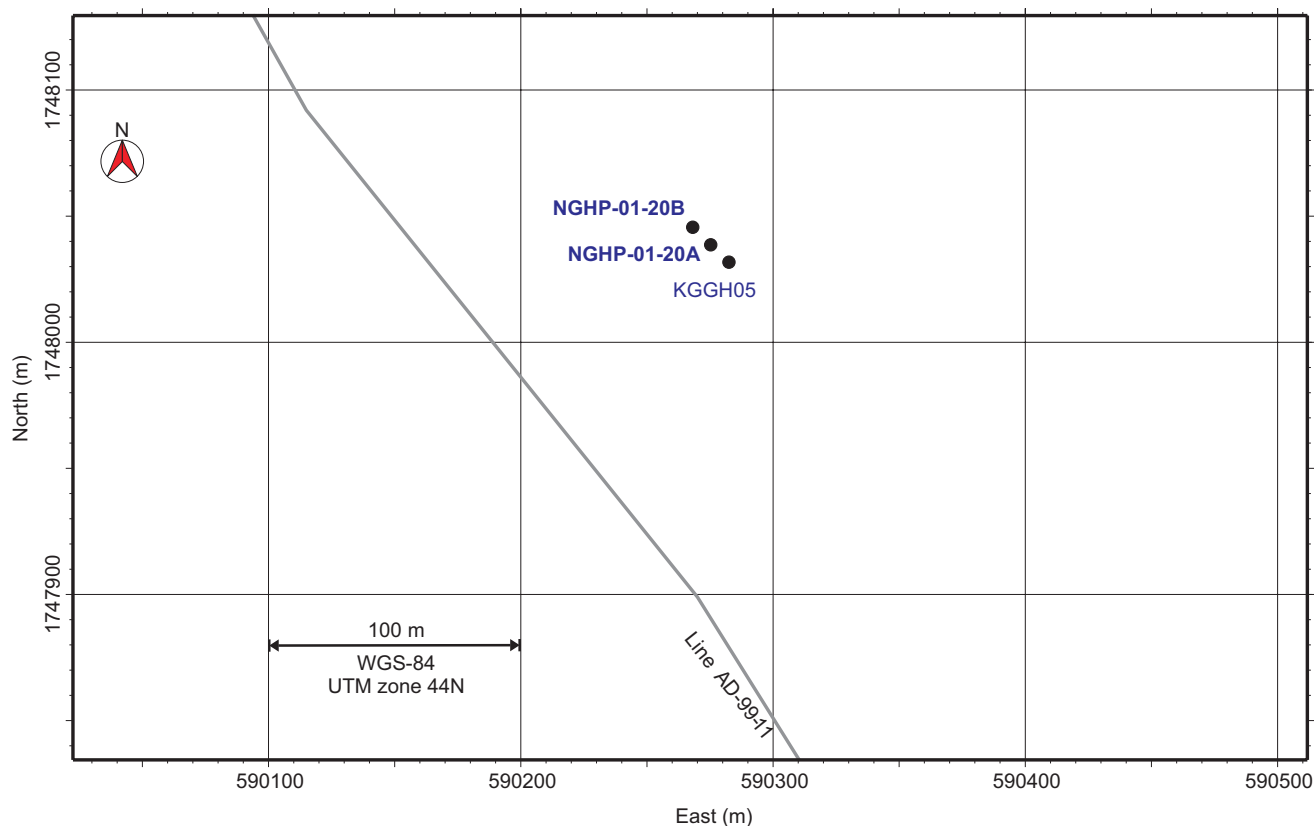


Figure 3. Map showing all holes occupied at Site NGHP-01-20 (KGGH05).

At 1845 hr, a PCS core was cut from 147.8 mbsf to 148.8 mbsf. However, the tool failed to actuate properly and only 57 cm of non-pressurized core were recovered.

Prior to attempting to deploy the FPC and HRC pressure coring systems, it was deemed essential that additional remedial hole conditioning be done. Three hours were spent attempting to improve the condition of the hole to an acceptable level for the planned pressure coring. This was to no avail and at 2330 hr on 11 August the decision was made to abandon Hole NGHP-01-20A and prepare for spudding a second hole at this site. Although the operational problems in Hole NGHP-01-20A were considered to be formation related it was hoped that a second hole might have a better chance of satisfying the objectives for the site. The hole was displaced with 60 bbl of 10.5 ppg Sepiolite mud and the drill string was pulled clear of the seafloor at 0040 hr on 12 August. This ended operations in Hole NGHP-01-20A and began Hole NGHP-01-20B.

In Hole NGHP-01-20B, penetration rates with the XCB ranged from 12.8 m/h to 38.4 m/h and core recovery with the XCB system was extremely variable, ranging from 3 percent to 102 percent.

Whirlpaks (microbeads) commonly used for assessing microbiological contamination were not used for coring. Accelerated core barrel handling protocols were used for all core barrels (APC, XCB, and PCS) deployed in this hole. All APC/XCB core barrels were laid down immediately upon arrival at the rig floor before making another drill pipe connection or deploying the next core barrel.

Hole NGHP-01-20B

The vessel was offset 10 m NW of Hole NGHP-01-20A and the drill string was spaced out for spudding. A center bit was deployed and Hole NGHP-01-20B was spudded at 0115 hr on 12 August. Seafloor depth was considered to be 1,157.9 mbrf; the same as that of Hole NGHP-01-20A. Drilling continued in this hole to a depth of 148.8 mbsf at an average ROP of 22.0 m/h. A 20 bbl Sepiolite mud sweep was pumped and the XCB center bit was recovered. XCB Core NGHP-01-20B-1H was on-deck at 0915 hr and coring continued through Core NGHP-01-20B-4X to a depth of 187.3 mbsf. A decision was made to abandon this hole at 1200 hr on 12 August due to problems with hole stability that were similar to those experienced in Hole NGHP-01-20A, including: poor core quality and recovery, poor hole condition, and packing-off. A general consensus was reached that neither pressure cores nor wireline logs would be recoverable from the hole. Penetration rates with the XCB ranged from 38.4 m/h to 57.6 m/h and core recovery with the XCB system ranged from 0 percent to 17 percent.

Whirlpaks (microbeads) commonly used for microbiological contamination control were not used in Hole NGHP-01-20B. Accelerated core barrel handling protocols were used for all core barrels (APC, XCB, and PCS) deployed in this hole. All APC/XCB core barrels were laid down immediately upon arrival at the rig floor before making another drill pipe connection or deploying the next core barrel.

The hole was abandoned with 60 bbl of 10.5 ppg Sepiolite mud. The drill string was pulled clear of the sea-floor at 1345 hr. The beacon was recovered at 1504 hr during the remaining pipe trip to the surface. The drill collars were racked back in the derrick and the vessel was secured for transit by 1630 hr on 12 August. This ended operations for Hole NGHP-01-20B as well as for Site NGHP-01-20.

Lithostratigraphy

Site NGHP-01-20 is located in the Krishna-Godavari (KG) Basin, along the eastern continental margin of India, ~100 m downslope of Sites NGHP-01-10–12 and -21. At Site NGHP-01-20, two holes (NGHP-01-20A and NGHP-01-20B) were drilled and cored, one to a depth of 187.3 mbsf; Hole NGHP-01-20A was cored to 147.8 mbsf and Hole NGHP-01-20B was drilled to 148.8 mbsf, then cored from 148.8 mbsf to 187.3 mbsf. Pressure coring and wireline logging were not attempted due to poor hole conditions experienced in both Holes NGHP-01-20A and NGHP-01-20B (see “Operations”).

We classified the sedimentary sequence recovered at Holes NGHP-01-20A and NGHP-01-20B as one lithostratigraphic unit (Unit I) based on sedimentological criteria (for example, variations in sedimentary structures and grain size or biogenic and lithogenic components) and physical properties (for example, magnetic susceptibility; see fig. 4 and “Site NGHP-01-20 Visual Core Descriptions”). We also integrated the core data with the available seismic data to help define and interpret the stratigraphic section cored at Site NGHP-01-20. Based on the limited core recovery in both Holes NGHP-01-20A and NGHP-01-20B, it is difficult to directly correlate the recovered record with the other sites in the KG Basin; however, the downcore magnetic susceptibility appears consistent with the pattern observed at the other KG Basin sites. The lack of *Discoaster spp.* at this site, also leads us to suspect that the stratigraphy recovered at Site NGHP-01-20 is Quaternary in age and may be equivalent to the uppermost KG Basin stratigraphy recovered at other sites. Postcruise biostratigraphy, however, may help tie the record recovered at Site NGHP-01-20 with the other KG Basin sites.

Lithostratigraphic Units

Lithostratigraphic unit I

Intervals: Hole NGHP-01-20A,
Sections NGHP-01-20A-01H-1 to
-20P-CC and Hole NGHP-01-20B,
Sections NGHP-01-20B-01X-1 to -04X-CC.

Depth: Hole NGHP-01-20A, 0–148.8 mbsf;
NGHP-01-20B, 148.8–187.3 mbsf

Age: Quaternary

Core recovery at Hole NGHP-01-20A from the APC cored interval between 0 to ~23 mbsf was generally good; below ~23 mbsf, recovery was extremely low, except for

Core NGHP-01-20A-16X, which was fully recovered (fig. 4 and “Site NGHP-01-20 Visual Core Descriptions”). As inferred from the porewater chemistry and sedimentological data collected at Hole NGHP-01-20A (see “Inorganic Geochemistry”), core recovery was likely limited due to the presence of coarse lithologies and/or abundant gas hydrate. Lithostratigraphic Unit I is composed of a variety of nannofossil-bearing to -rich clay, volcanic glass-bearing to -rich clay, pyrite-bearing to -rich clay, and authigenic carbonate-bearing to -rich clay. The sediments range in color from dark grayish brown (10Y 4/2) to very dark grey (10YR 3/1) to black (N 2.5/1 or 5Y 2.5/1; see figs. 4 and 5 and “Site NGHP-01-20 Visual Core Descriptions”). Sand and silt laminae and beds as well as thicker zones of silty clay are present throughout the recovered sequence (figs. 4 and 5 and “Site NGHP-01-20 Visual Core Descriptions”). Although the core recovery was less at Site NGHP-01-20 compared to the other KG Basin sites, the amount of silt-sized grains observed in smear slides was greater and the occurrences of sandy and silty clay intervals were more pronounced at this site (figs. 4 and 5 and “Site NGHP-01-20 Visual Core Descriptions” and table 1). This is consistent with the position of Site NGHP-01-20 in slightly deeper water, which is perhaps more conducive to sand and silt deposition, compared to the other KG Basin sites.

Shell fragments and visible foraminifera tests occur sporadically throughout the Unit (figs. 4 and 6 and “Site NGHP-01-20 Visual Core Descriptions”). A spiny gastropod shell (2.5 cm at widest point) was recovered in Core NGHP-01-20A-17X (figs. 4 and 6B and “Site NGHP-01-20 Visual Core Descriptions”). Authigenic carbonates, present as bands, nodules (>1 cm), and micronodules (<1 cm) are common throughout the recovered stratigraphy of Unit I (figs. 4 and 7 and “Site NGHP-01-20 Visual Core Descriptions”). Although a distinct bed of ash was not observed within the recovered cores, detrital volcanic glass shards were observed in smear slides taken throughout the Unit. Glass shards are typically present as trace to 20 percent (table 1). Rare bioturbation occurred in the top ~23 mbsf; whereas below 23 mbsf bioturbation was not observed; however, this lower part of the core is coincident with the zone of XCB coring and bioturbation was difficult to determine in the disturbed XCB cores. Bioturbated zones are also most easily seen in lighter-colored portions of the cores where such zones are highlighted by dark grey to black colored iron sulfide precipitates. Identification of iron sulfides and pyrite, from visual observation in cores (fig. 4 and “Site NGHP-01-20 Visual Core Descriptions”), shows it is present only in Cores NGHP-01-20A-01H, NGHP-01-20A-02H, and NGHP-01-20A-16X; however, pyrite and other iron sulfides are present in coarse fractions (trace up to 30 percent) throughout the Unit (table 1).

Downcore magnetic susceptibility values (fig. 4) are moderately high throughout the unit, except for the interval between 4 mbsf and 10 mbsf, which is anomalously low. The magnetic susceptibility pattern at the top of the hole (0 mbsf to ~22 mbsf), where the recovery is good, is similar to that observed in the upper stratigraphy throughout the KG Basin. This pattern is likely caused by systematic variation in the

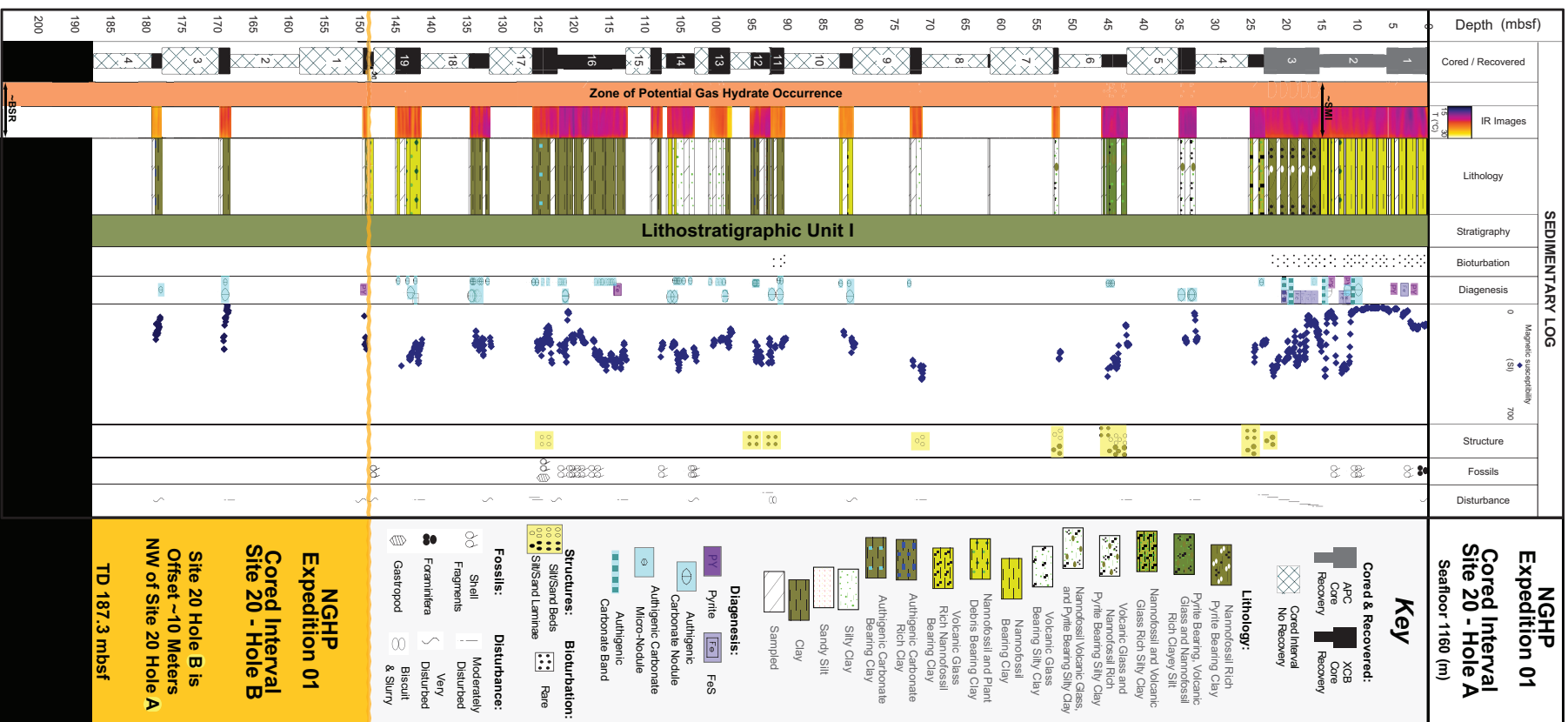


Figure 4. Lithostratigraphic summary of Holes NGHP-01-20A and NGHP-01-20B. [BSR, bottom-simulating reflector; SMI, sulfate-methane interface] Note: Colored intervals exceed symbol size when there is a range in the occurrence. The center point of each symbol represents depth of occurrence; therefore, colored bars may slightly exceed core recovery; see Site NGHP-01-20 Visual Core Descriptions for the expanded scale, detailed core descriptions; see Site NGHP-01-20 Oversized Figure for the enlarged version of this summary.

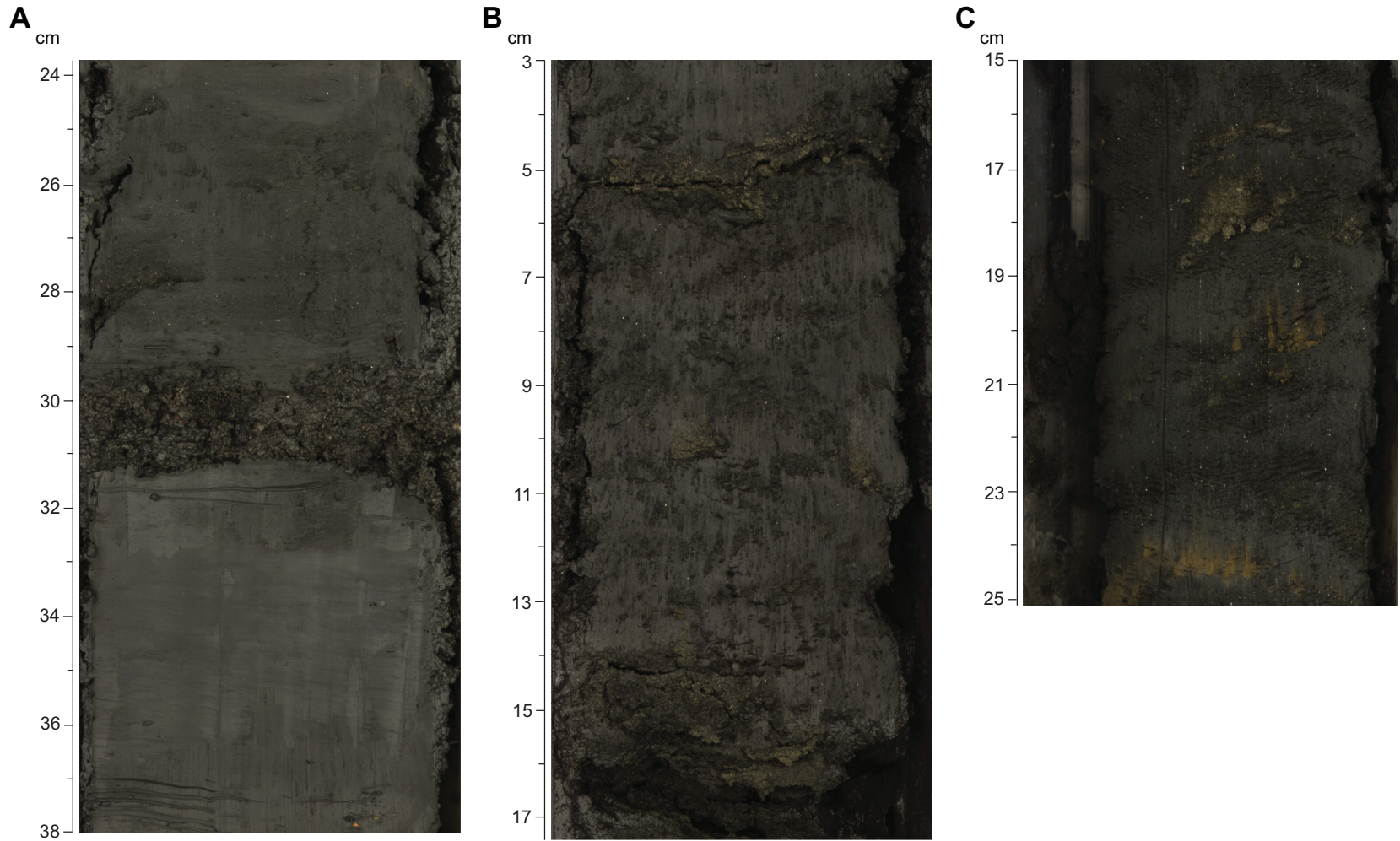


Figure 5. Sand and silt laminae and beds. A, Section NGHP-01-20A-04X-2, 24–38 cm; B, Section NGHP-01-20A-06X-4, 3–17 cm; C, Core NGHP-01-20A-11X-2, 15–25 cm. Also notice the authigenic carbonate precipitates.

Table 1. Smear-slide data for Holes NGHP-01-20A and NGHP-01-20B.

Sample reference			Texture					Mineral									
Core, section, depth (cm, in section)	MBSF	Lithology	Sand	Silt	Clay	Quartz	Feldspar	Mica	Heavy minerals	Clay minerals	Volcanic glass	Glauconite	Framboidal pyrite	Iron sulfides	Rock fragments	Authigenic carbonates	
NGHP-01-20A																	
1H-1,80	0.80	D		5	95	2		1	2	76	2			3		1	
1H-2,50	2.00	D		1	99	2			2	81	trace			3		trace	
1H-3,40	3.40	D		5	95	3			1	80	2			2		trace	
2H-2,70	7.80	D		7	93	2		trace	1	75	4			3		1	
2H-4,42	10.52	D		2	98	2			1	84	2			1		1	
2H-5,70	12.30	D		15	85	5			2	67	4			3		1	
2H-7,2	14.12	D		5	95	3			1	81	3			2		1	
3H-2,50	17.10	D		20	80	10	2	2		39	3	1	7			2	
3H-3,10	18.20	M		15	85	8	2	3		39	2			3			
3H-5,66	21.76	M		40	60	15	3	2		50	2	2	trace	2		1	
4X-2,35	24.75	D		10	90	4	trace	trace	2	62	7			2		trace	
4X-2,28	24.68	M		2	30	68	20	2		44	9	trace	trace	3		1	
4X-cc,unk	unk	M	40	40	20	50	10	1	7	20	trace	2		3		trace	
5X-2,30	34.30	D		2	28	70	2	trace	trace	52	15	1		3			
6X-2,36	43.96	D		5	50	45	10	2	trace	48	20	trace	6			1	
7X-1,28	51.98	D		2	28	70	20	trace	trace	54	8	1		5			
9X-2,10	72.50	D			30	70	15	1	trace	66	10	1		3		trace	
10X-1,25	80.85	D			15	85	5	trace	trace	69	11	1		3			
11X-1,50	90.70	D	1	5	94	5		2		89							
11X-2,14	91.84	M	10	85	5	90	2		5	2	1			trace		trace	
12X-2,53	94.23	D		5	95	2				65	1					30	
13X-2,35	99.37	D		2	98	5	2			84						5	
14X-2,35	104.65	D	5	35	60	10	1	trace	3	78	trace			1		4	
14X-3,25	106.05	D		2	98	5			1	85						3	
15X-1,36	107.76	D		15	85	10	1		3	82	trace			2			
16X-2,80	114.70	D		15	85	7	2		trace	87	trace					3	
16X-5,60	189.00	D		7	93	8	1		1	88						1	
17X-2,35	123.45	D		5	95	5			2	87				1		5	
17X-2,67	123.77	M	10	87	3	92	1		5		trace			trace			
18X-2,30	132.90	D		15	85	3			3	83	2					1	
19X-2,25	142.95	D		20	80	7	2	1	3	69	2			2		1	
20P-1,50	148.30	D		20	80	7			3	71	2		trace	4			
NGHP-01-20B																	
1X-1,30	149.10	D		2	98	3	trace	trace	2	89	1					3	
3X-1,90	169.00	D		3	97	5			1	92				trace		trace	
4X-1,66	178.36	D		5	95	5				54						40	

amount of magnetic minerals. This variation may be due to primary deposition or secondary Iron-Sulfur (Fe-S) diagenesis (for example, see “Lithostratigraphy” in “Site NGHP-01-14”). However, the lack of sand and silt beds, which generally contain abundant detrital magnetite grains, and the abundance of iron sulfides from 0 mbsf to ~22 mbsf suggest that the susceptibility signal in this region may be diagenetic. Magnetic iron sulfides (likely gregite and/or pyrrhotite) have been observed in gas hydrate bearing sediments offshore western North America (Musgrave and others, 2006) and at some of the KG Basin sites cored during NGHP Expedition 01 (for example, see “Lithostratigraphy” in “Site NGHP-01-03”) and may be responsible for some of the magnetic susceptibility highs observed here. However, subtle changes in detrital magnetic mineral grains present in the more clay-rich (biogenic-poor) zones may also explain some of this subtle variability.

The major lithologies of Lithostratigraphic Unit I determined from smear slides consist primarily of clay-sized grains (45–99 percent) with a greater amount of silt-sized

grains (up to 50 percent in the silty clay intervals) than seen at other KG Basin sites (table 1 and fig. 8B). Minor lithologies described in smear slide included burrow fills, anomalous lighter colored clay regions, and sand and silt beds (table 1). The major non-biogenic components described in smear slides and coarse fractions in Lithostratigraphic Unit I are quartz, feldspar, mica, heavy minerals, iron sulfides, pyrite, clay minerals, and volcanic glass fragments (table 1 and fig. 8C). Smear slides show glauconite and authigenic carbonates are also present throughout much of Site NGHP-01-20 (table 1). The total biogenic component of the sediment, as learned from smear slides, is dominated by calcareous nannofossils, which comprise trace to 40 percent of all sediment grains, foraminifera (up to 2 percent) and other calcareous shell fragments (2–4 percent; table 1 and fig. 8C). In coarse fractions (>63 μm), foraminifera are present (10 to 50 percent) and together with other calcareous shell fragments (5–65 percent) dominate the calcareous biogenic component (table 2 and fig. 8C). Foraminifera are often visible with the naked eye on

Table 1. Smear-slide data for Holes NGHP-01-20A and NGHP-01-20B.—Continued

Sample reference Core, section, depth (cm, in section)	Biogenic								Comments
	Fora- minifera	Nanno- fossils	Carbonate shell fragments	Diatoms	Radio- larrians	Silico- flagellates	Sponge spicules	Plant debris	
NGHP-01-20A—Continued									
1H-1,80	trace	10					trace	3	
1H-2,50	1	7						4	
1H-3,40	2	7						3	
2H-2,70	trace	8	2	trace			trace	4	microtektites present
2H-4,42	trace	7		trace				2	
2H-5,70	1	7	4					6	
2H-7,2	trace	7						2	from lighter clay, pyrite is cubic, botryoidal and pyritahedrons
3H-2,50		30						4	
3H-3,10		40						3	from FeS zone, mica is chlorite and biotite
3H-5,66	1	20						2	from silty zone, forams altered
4X-2,35	1	20						2	trace amphibole
4X-2,28		20						1	from sandy/silt zone
4X-cc,unk		5				trace		2	very coarse grained; trace amphibole, mica is biotite
5X-2,30	1	20						2	trace amphibole
6X-2,36	trace	11						2	trace amphibole
7X-1,28	trace	10						2	trace amphibole
9X-2,10		3						1	trace amphibole
10X-1,25	1	8						2	trace amphibole
11X-1,50	trace	1						1	
11X-2,14							trace		from sand layer, trace amphibole
12X-2,53								2	
13X-2,35		trace						2	
14X-2,35	trace	trace						3	from silty/sandy clay
14X-3,25		5						1	
15X-1,36	2	trace							forams are mostly broken tests
16X-2,80		trace						1	
16X-5,60	trace	trace						1	trace amphibole
17X-2,35									trace rutile
17X-2,67	2								from sand
18X-2,30		3	2					3	
19X-2,25	2	5						6	
20P-1,50	1	5						7	
NGHP-01-20B									
1X-1,30	trace							2	
3X-1,90	2	trace							
4X-1,66								1	

Note: M = minor lithology, D = dominant lithology

the split core surfaces as well. Detrital volcanic glass is also present in both the coarse fractions and the smear slides and is most abundant from 20 mbsf to 50 mbsf (fig. 8C). Terrestrial organic matter is also common (1 to 7 percent) in smear slides taken throughout Unit I (table 1 and fig. 8C) and present in trace amounts in the coarse fraction.

Gas Hydrate Occurrence

At Site NGHP-01-20A, the entire cored interval was above the level of the BSR and thus most likely within the zone of potential gas hydrate occurrence. No moussey texture was observed in the split cores from Site NGHP-01-20. Several thin IR anomalies, however, as well as several chlorinity anomalies were observed in the cores which may indicate the presence of gas hydrate (see “Inorganic Geochemistry” and “Physical Properties”). The sediments from the core intervals associated with these anomalies may provide additional insights into the nature of the hydrate accumulations.

The shallowest IR anomaly was recorded at ~43 mbsf and occurred coincident with a pyrite-bearing, volcanic glass and nannofossil rich clayey silt containing several coarser grained silt and sand beds and laminae. A second IR anomaly, detected between 115 mbsf and 125 mbsf (see “Physical Properties”), was associated with a fine-grained clay containing no silt, sand beds, or laminae. The IR anomaly at this interval appears to be broader and more diffuse than the more discrete anomaly observed at ~43 mbsf and may reflect a more disseminated accumulation of gas hydrate in this finer grained material. Porewater geochemistry data showed freshening at 82 mbsf within a volcanic-glass rich, nannofossil-bearing clay. However, no coarser grained silt, sand beds, or laminae were observed in the split cores, nor was any IR anomaly observed over this interval (table 3). At present, the relationship between the lithologic, porewater chemistry, and IR anomaly data are not easily resolved as no pressure cores or wireline logging data were collected at Site NGHP-01-20 due to poor borehole conditions.

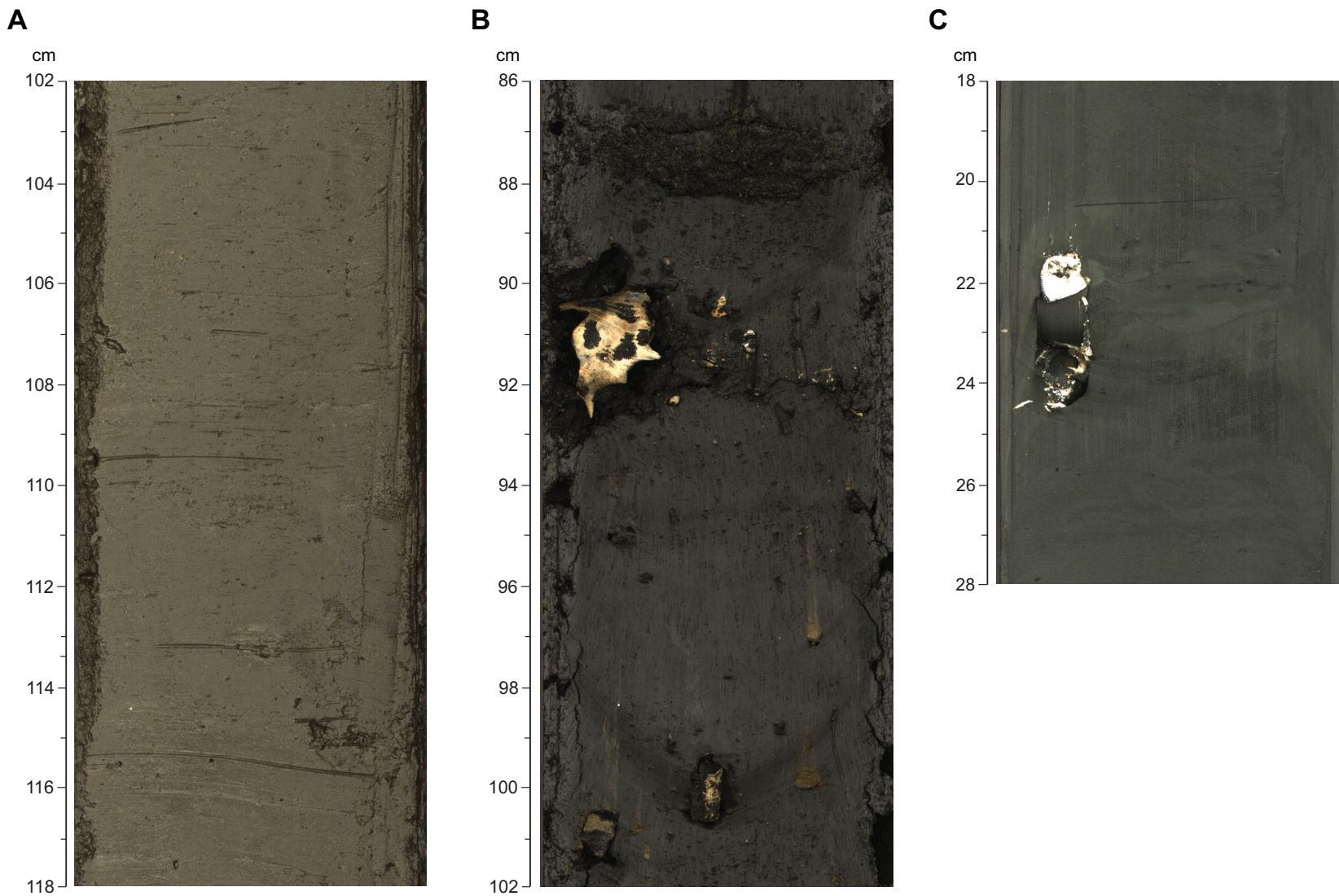


Figure 6. A, Visible foraminifera; and B and C, shell fragments observed throughout Unit I. A, Section NGHP-01-20A-01H-2, 102–118 cm; B, Section NGHP-01-20A-17X-2, 86–102 cm (also notice the authigenic carbonate micronodules); C, Section NGHP-01-20A-02H-4, 18–28 cm.

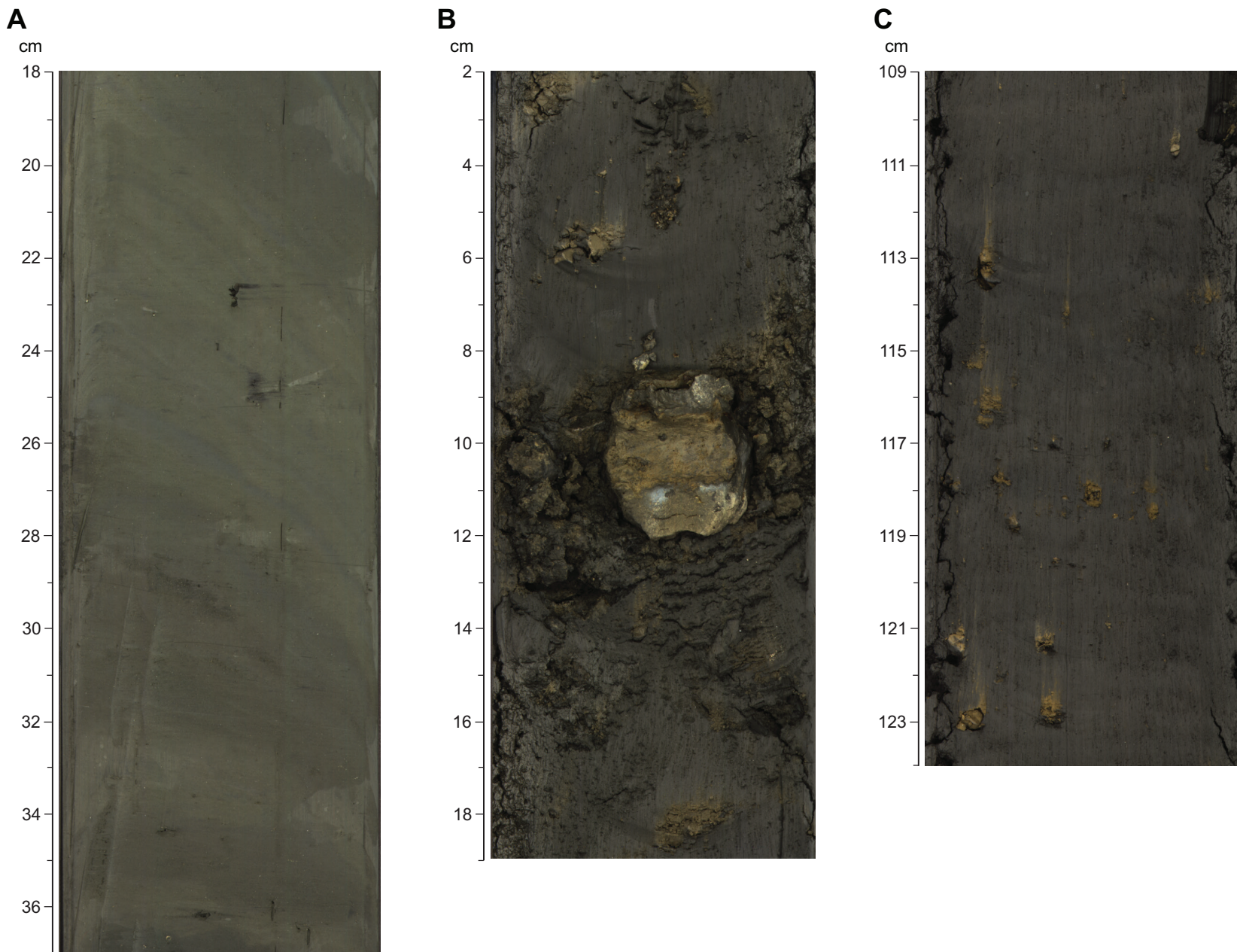


Figure 7. Authigenic carbonate occurrences in Unit I. A, lighter colored bands with fine grained precipitates, Section NGHP-01-20A-02H-07, 18–37 cm; B, nodules (>1 cm), Section NGHP-01-20A-16X-8, 2–19 cm; C, micronodules (<1 cm), Section NGHP-01-20A-17X-2, 109–124 cm.

A Holes NGHP-01-20A and B - Summary of major lithologic components

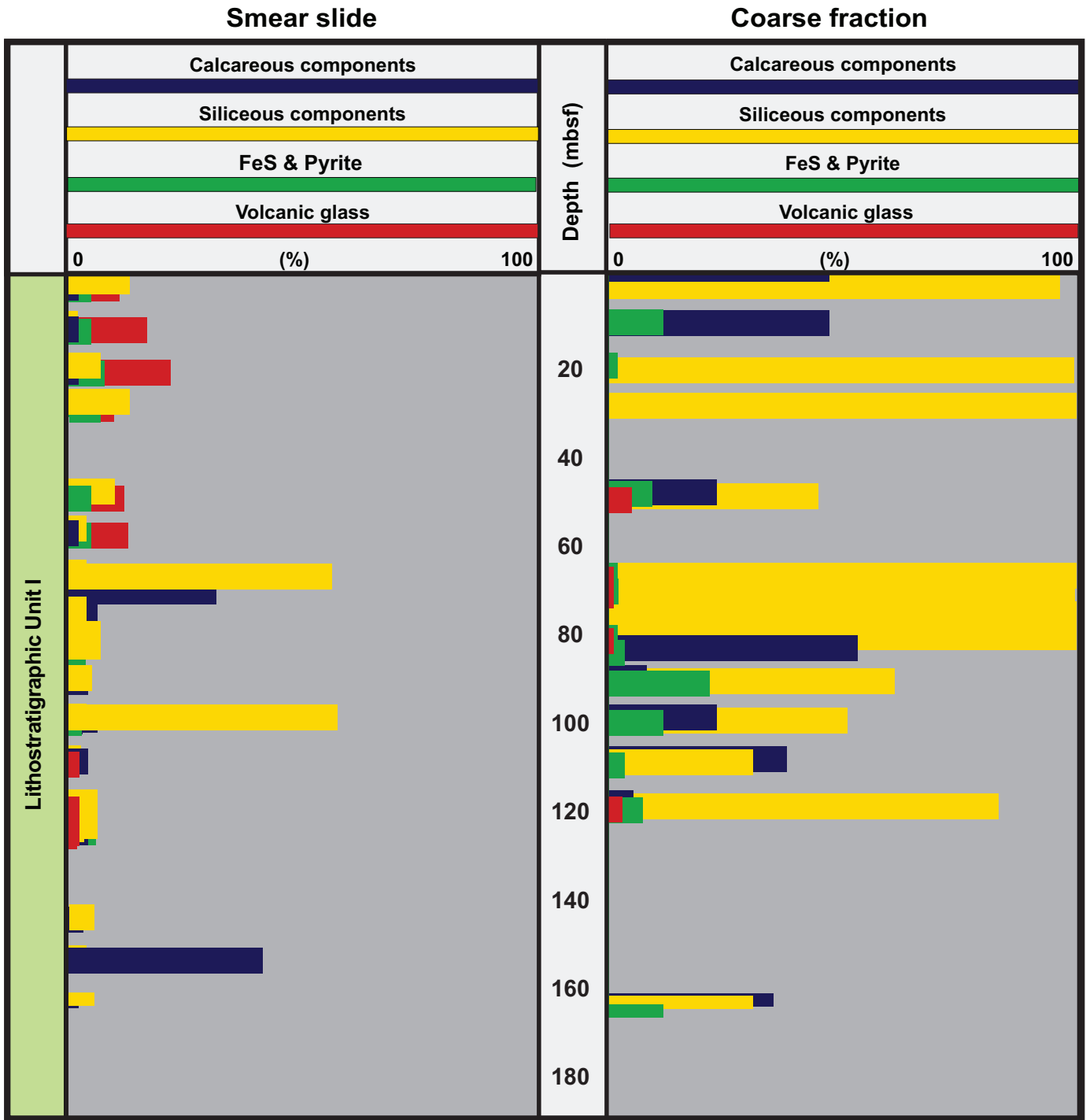


Figure 8. A, Summary of the major lithologic components in smear slides (see table 1) and coarse fraction data (see table 2) plotted from percent visual estimation. B, Major lithologic components in coarse fraction and smear slide; shown for clarity as individual abundance plots. C, Grain size distribution determined from smear slide sand, silt, and clay percentage estimations. (Some vertical overlap between the data bars is a result of the condensed vertical scale of the plots.)

B

Holes NGHP-01-20A and B - Smear slide based grain size distribution



Figure 8. A, Summary of the major lithologic components in smear slides (see table 1) and coarse fraction data (see table 2) plotted from percent visual estimation. B, Major lithologic components in coarse fraction and smear slide; shown for clarity as individual abundance plots. C, Grain size distribution determined from smear slide sand, silt, and clay percentage estimations. (Some vertical overlap between the data bars is a result of the condensed vertical scale of the plots.)—Continued

C Holes NGHP-01-20A and B - Smear slide and coarse fraction components

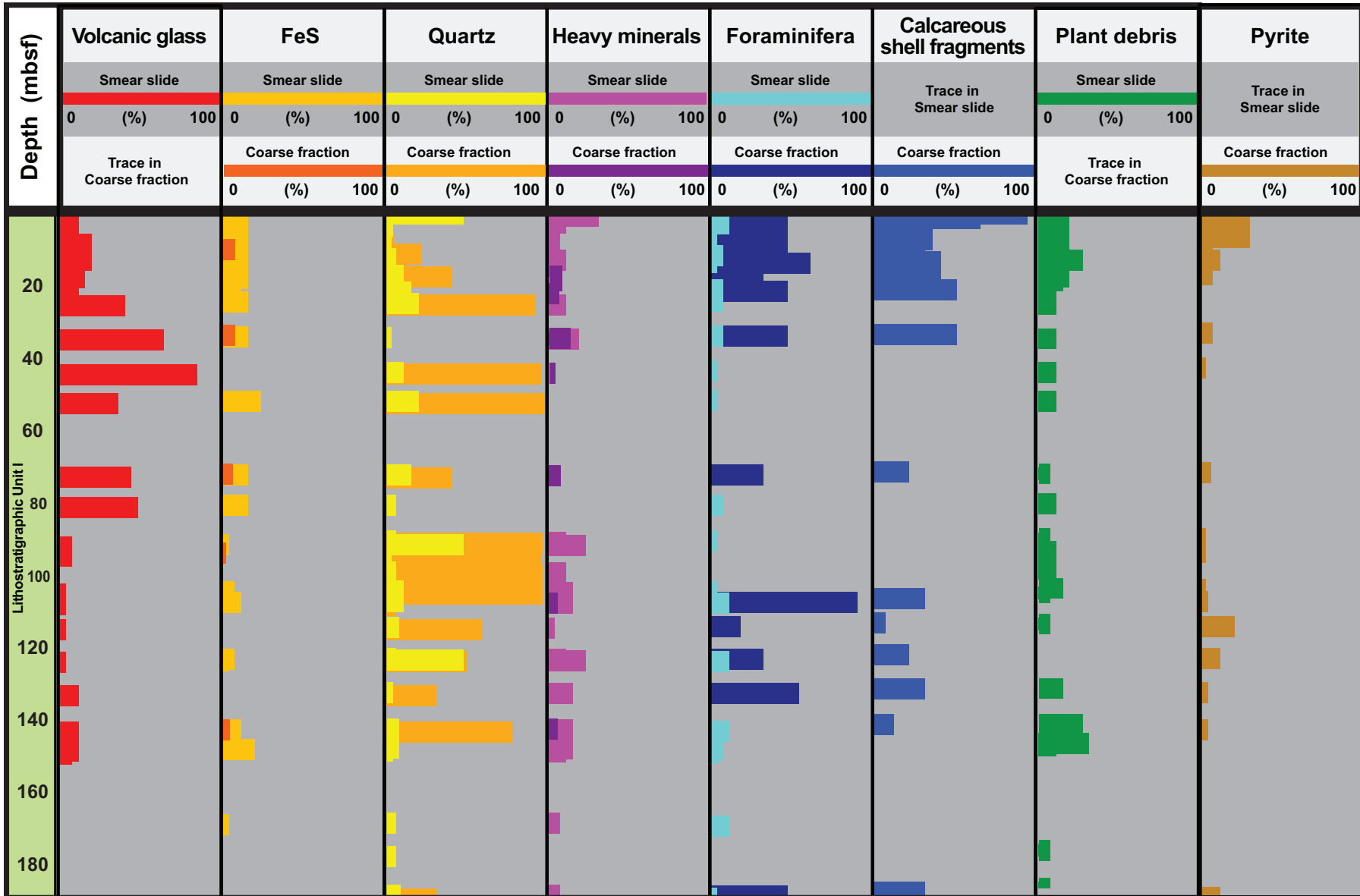


Figure 8. A, Summary of the major lithologic components in smear slides (see table 1) and coarse fraction data (see table 2) plotted from percent visual estimation. B, Major lithologic components in coarse fraction and smear slide; shown for clarity as individual abundance plots. C, Grain size distribution determined from smear slide sand, silt, and clay percentage estimations. (Some vertical overlap between the data bars is a result of the condensed vertical scale of the plots.)—Continued

Inorganic Geochemistry

Site NGHP-01-20 was drilled in the KG Basin to evaluate the gas hydrate distribution and abundance in this location. Site NGHP-01-20 is located ~3.5 km SE of Site NGHP-01-10, which contained massive gas hydrate. At Site NGHP-01-20 two holes, located ~10 meters apart, were cored. Hole NGHP-01-20A was terminated at 149 mbsf, when hole conditions prevented further drilling; Hole NGHP-01-20B was washed to 148 mbsf, and four additional XCB cores were raised from this site with very poor recovery in the first two cores. Only two interstitial water (IW) samples from Cores NGHP-01-20B-3X and NGHP-01-20B-4X were processed for analyses. Important goals of the inorganic geochemistry program at Site NGHP-01-20 are to constrain the hydrological and biogeochemical characteristics of the Krishna-Godavari Basin, especially in the vicinity of Site NGHP-01-10, which has abundant gas hydrate, and to identify and quantify the fluid and gas source(s). A comparative study of the structure, lithology, and geochemistry between Sites NGHP-01-20 and NGHP-01-10 may provide valuable insights on the regional controls on gas hydrate distribution and concentration. The IW chemical data are tabulated in tables 4 and 5 and illustrated in figures 9, 10, and 11.

A total of thirty-four samples in Hole NGHP-01-20A and two samples in Hole NGHP-01-20B were collected and processed for IW analyses, in coordination with both the organic geochemistry and microbiology sampling programs. Only conventional cores were obtained at this site (no pressure cores). Whole-round lengths ranged from 10 to 30 cm, with longer sections sub-sampled from cores recovered deeper in the hole. In the upper 20 mbsf at Hole NGHP-01-20A, thirteen whole, round samples were collected to constrain the SMI and provide supporting data and samples for studies on the microbial dynamics of the SMI. In the first three cores, IW samples were obtained from each section. Only one sample was collected per core from Core NGHP-01-20A-04X to TD because of rather poor core recovery. The only exceptions were Cores NGHP-01-20A-06X and NGHP-01-20A-16X, which showed anomalies in the IR scans and thus two samples were collected from each core. The IW samples with an IR anomaly were immediately transferred to a photography station specially prepared for handling, imaging, and recording observations related to gas hydrate occurrence. After characterization by IR and visible photography, the sample was split into a IR inferred colder and a background sample that were squeezed and analyzed separately. No lithological differences were observed between the IR anomaly and background intervals in these two sediment samples. Note that XCB drilling was required to obtain the fourth core, at a depth of just ~24 mbsf. The sediment was very fine grained, dark brown to black compacted clay that was difficult to clean and squeeze. Therefore, even after thoroughly cleaning, the extent of sulfate

contamination by drill water was considerably higher than usual, as recorded in table 4. The data corrected for drillwater contamination based on sulfate are presented in table 5 and plotted in figures 9, 10, and 11.

Interstitial Water Chloride and Salinity

Chloride concentration was determined by titration with AgNO_3 , with an average percent deviation of 0.2 percent, and salinity was determined by refractometry. The chloride concentration and salinity data are presented in table 5 and illustrated in figure 9.

The salinity depth profile shows a steady decrease with depth from about 34.5 to a minimum salinity of ~29 at the bottom of both Holes NGHP-01-20A and NGHP-01-20B (fig. 9B). In the uppermost ~25 mbsf, the rapid decrease in salinity reflects the diagenetic loss of sulfate and most likely some of the major seawater cations, primarily Ca^{2+} and Mg^{2+} , by biogeochemical reactions that induce authigenic carbonate formation. Deeper in the section, salinity mostly mimics the Cl^- profile (fig. 9C) with minima between ~45 and 118 mbsf. The lowest salinity values were measured in one of the IR anomaly samples (Core 6X, at 45 mbsf) and in Sample 20A-14X-1, 125–150m (104 mbsf). The corrected salinity values for these samples are 27.5 and 27.7, respectively. The discrete low salinity values at this depth interval coincide with low Cl^- values (table 5 and fig. 9) and indicate the presence of gas hydrate in these sediments.

Against a background salinity of ~31.5 in this depth range, these data (presented in table 5) suggest dilution by gas hydrate dissociation of ~13 percent.

The Cl^- depth profile also shows a constant concentration, 558 ± 1 , from the seafloor to ~22 mbsf. Below this depth, there is a steady decrease in the background Cl^- to a minimum value of 544 (97 percent of the shallow value) at the bottom of Hole NGHP-01-20A and 513 (~92 percent of the shallow value) at the bottom of Hole NGHP-01-20B (fig. 9B). This decrease was probably caused by dissociation of small amounts of finely dispersed gas hydrate, which slightly increased in abundance with depth. The decrease in the background Cl^- value coincides with the change in coring mode from APC to XCB. Most of the samples recovered below ~45 mbsf to 118 mbsf show significant dilution relative to the local background values, and represent dissociation of larger concentrations of gas hydrate during core recovery operations (table 5). The lowest Cl^- values measured within this depth interval are 471 and 475 mM at 45 and 82 mbsf, respectively, corresponding to ~16 percent seawater dilution. It is interesting to note that below ~118 mbsf to TD of ~179 mbsf in Hole B, situated ~40 meters above the seismic BSR, only background Cl^- and salinity values were recorded. The absence of IR anomalies in the deepest ~60 mbsf drilled at this site may reflect sparse sediment recovery in this depth interval.

Table 2. Coarse fraction (>63 µm) sieve data for Holes NGHP-01-20A and NGHP-01-20B.

Sample reference		Mineral											
Core, section, depth (cm, in section)	MBSF	Quartz	Feldspar	Mica	Heavy minerals	Volcanic glass	Pyrite	Iron sulfides	Fram-boidal pyrite	Rock fragments	Pumice	Other minerals	Authigenic carbonates
NGHP-01-20A													
1H-1,80	0.8												
1H-2,50	2												
1H-3,40	3.4						30		30				
2H-2,70	7.8	2					30						
2H-4,42	10.52	20		10			5	5					
2H-5,70	12.3	10		20			5						
2H-7,2	14.12	2		3			10						
3H-2,30	16.9	40		5	5								
3H-3,10	18.2			5	5		5						
3H-5,66	21.76			5	3							2	
3H-cc,unk	unk	95	trace	3	2								
4X-2,30	24.7	95	3									2	
5X-2,30	34.3				10		5	5					
6X-2,27	43.87	98	0.5	0.5	0.5		0.5						
7X-1,28	51.98	100	trace	trace	trace								
9X-2,10	72.5	40		4	4	4	4	4					
10X-1,25	80.85	95										2	
11X-1,50	90.7	99	0.2	0.2	0.2	0.2	0.2	trace	trace	trace		trace	trace
12X-2,53	94.23	98	0.2	0.2	0.2	0.2	0.2	0.2	0.2	0.2		0.2	0.2
13X-2,35	99.37	99										1	
14X-2,35	104.65	99	0.2	0.2	0.2	0.2	0.2	trace	trace	trace		trace	trace
15X-1,56	107.96	3		trace	2		2					3	
16X-2,80	114.7	60					20					5	
16X-5,60	189	30					10						
17X-2,35	123.45	50					10						
18X-2,30	132.9	30					2						
19X-2,25	142.95	80		trace	2	2	2	2	2				
NGHP-01-20B													
1X-1,30	149.1	40					40	10					
3X-1,40	168.5	55					2	3					
4X-1,66	178.36	90	trace	trace				trace					10

Sulfate and Alkalinity Concentrations: Characterization of the SMI

The primary objectives of the higher resolution sampling in the upper 20 m of the sediment section were to delineate and characterize the sulfate-methane interface (SMI) for future geochemical modeling of methane fluxes and to provide supporting data and samples for studies on the microbial dynamics of the SMI. At Site NGHP-01-20, the SMI is located at ~15 mbsf (fig. 10B), which is at shallower depth than at most sites drilled in the KG Basin, except for Hole NGHP-01-03C, where the SMI depth is at ~9 mbsf, and at Hole NGHP-01-05D, where it is at ~10 mbsf. At the other KG locations drilled (NGHP-01-03B, NGHP-01-05C, NGHP-01-07, NGHP-01-10, NGHP-01-12, NGHP-01-14, NGHP-01-15, and NGHP-01-16), the SMI depths are between 20 and 25 mbsf. Because the dissolved sulfate gradient is an approximate proxy for upward methane flux in continental margins, and particularly at gas hydrate sites, it is conspicuous that the SMI at Sites NGHP-01-10 and NGHP-01-12 (with massive gas hydrate) is deeper than at Site NGHP-01-20 (with disseminated gas hydrate). This may indicate that the gas hydrate occurrence at Site NGHP-01-20 is controlled by lithology, whereas at

Sites NGHP-01-10 and NGHP-01-12 it is fracture controlled. The methane concentrations measured at this site are low with only a small maximum between ~18 to 25 mbsf. Such low concentrations, which are lower than those measured at other sites in the KG Basin, are most likely due to poor core quality and significant gas loss during recovery (see “Organic Geochemistry”). Based on the depth of the SMI, the methane concentrations should have been considerably higher than observed.

Alkalinity shows a broad maximum from 16 to ~45 mbsf, where it reaches 21.3 mM (fig. 10A). This distribution reflects the combined effects of SO_4^{2-} reduction (associated with organic matter decomposition), anaerobic methane oxidation, carbonate precipitation, and carbonate dissolution driven by methanogenesis. The alkalinity depth profile suggests authigenic carbonate formation, particularly at the depth of the alkalinity maximum, but also possibly deeper in the sediment section where alkalinity values decrease. Although carbonate micro-nodules were present in the deeper sediment samples, their formation depth is unknown. The sulfate reduction profile is non-linear, particularly in the uppermost ~7 mbsf, reflecting that more than one SO_4^{2-} reduction reaction may control this profile. The profile will be modeled and utilized to compute

Table 2. Coarse fraction (>63 μm) sieve data for Holes NGHP-01-20A and NGHP-01-20B.—Continued

Sample reference	Biogenic										Comments
	Core, section, depth (cm, in section)	Foraminifera	Carbonate shell fragments	Diatoms	Radiolarians	Silico-flagellates	Siliceous shell fragments	Sponge spicules	Fish remains	Other biogenic	
NGHP-01-20A—Continued											
1H-1,80		95							5		fish remains are fecal pellets
1H-2,50	30	65							5		fish remains are fecal pellets
1H-3,40	20	15							5		
2H-2,70	30	35							3		fish remains are fecal pellets
2H-4,42	25	30							5		
2H-5,70	30	30						trace	5		
2H-7,2	40	40						2	3		
3H-2,30		30							20		
3H-3,10	20	40							25		
3H-5,66	30	50						trace	10		
3H-cc,unk											
4X-2,30											
5X-2,30	30	50									
6X-2,27											
7X-1,28											
9X-2,10	20	20							trace		
10X-1,25		3									
11X-1,50											
12X-2,53											
13X-2,35											
14X-2,35											
15X-1,56	60	30									
16X-2,80	10	5									other is a blackish mineral
16X-5,60	30	30									
17X-2,35	20	20									
18X-2,30	35	30						1	1	1	
19X-2,25		10							trace		
NGHP-01-20B—Continued											
1X-1,30		5							5		
3X-1,40	20	15	1	1	1	1			1		
4X-1,66											

the vertical component of the methane flux at this site. Below the SMI, SO_4^{2-} concentrations remain zero throughout the drilled section; the few slightly higher than 0.10 mM sulfate values, reported in table 4, most likely indicate contamination by drill-water. The most difficult samples to clean from drill-water contamination were the XCB cores, which were highly disturbed due to the properties of the formation. The sulfate concentrations in these samples were used to calculate the amount of drill-water contamination, and the salinity, alkalinity, Cl^- , and Br^- concentrations were corrected for the contamination. The corrected concentration values are listed in table 5.

Bromide Concentrations

Both the dissolved Br^- concentration and Br^-/Cl^- ratio depth profiles show only a minor increase in the upper 15 mbsf, suggesting that diffusive exchange with bottom seawater is slightly faster than production. Bromide concentrations and Br^-/Cl^- ratios then increase steeply to ~ 1.5 mM and 2.7×10^{-3} , at about 40 mbsf, reflecting decomposition of detrital marine organic matter (fig. 11). The maximum of 1.5 mM Br^- concentration is similar to concentrations observed at most other sites drilled in the KG Basin. Concentrations then scatter

between ~ 40 and 100 mbsf but do not increase with depth and remain rather constant to TD, suggesting no continued breakdown of marine organic matter with depth. This scatter is clearly related to gas hydrate decomposition as Br^-/Cl^- ratios vary smoothly with depth (fig. 11). Because the Br^- concentration-depth profiles provide insight into organic matter diagenesis and the type of organic matter, it is interesting to note that Br^- concentrations in the nearby Mahanadi Basin are somewhat lower than in the KG Basin. In the Andaman Basin, at Site NGHP-01-17, however, the values observed are higher.

Organic Geochemistry

Shipboard organic geochemical studies at Site NGHP-01-20 (KGGH-05) included analyses of the composition of volatile hydrocarbons including methane, ethane, and propane (C_1 – C_3) and fixed natural gases (that is, O_2 , CO_2 , and N_2 +Ar) from headspace only. In general, these analyses indicate that methane and CO_2 are the predominant gases found in the cores at Site NGHP-01-20. No hydrocarbons with higher molecular weights were present. The headspace samples from above the SMI were dominated by air and CO_2 . Methane was slightly enriched below the SMI and above the seismically-inferred

Table 3. Silt laminae and beds for Site NGHP-01-20.

Core section	Position start	Position end	Depth top (mbsf)	Depth base (mbsf)	Type
NGHP-01-20A					
3H-5	75	115	21.85	22.25	multiple silt laminae
4X-2	30	32	24.7	24.72	sand bed
4X-2	26	26	24.66	24.66	sand/silt laminae
4X-2	28	28	24.68	24.68	sand/silt laminae
6X-1	0	75	42.1	42.85	multiple silt/sand laminae
6X-2	0	100	43.6	44.6	multiple silt/sand laminae
6X-4	5	6	45.21	45.22	sand bed
7X-1	0	55	51.7	52.25	silty/sandy clay
7X-1	8	10	51.78	51.8	sand filled burrow
7X-1	37	37	52.07	52.07	thin sand/silt bed
7X-1	44	44	52.14	52.14	thin sand/silt bed
9X-1	0	75	70.9	71.65	silty clay
9X-2	5.5	5.5	72.455	72.455	sand filled burrow
9X-cc	0	70	72.68	73.38	silty clay
11X-1	9	9	90.29	90.29	sand filled burrow
11X-1	56	64	90.76	90.84	sand filled burrow
11X-1	73	75	90.93	90.95	sand filled burrow
11X-2	15	24	91.85	91.94	disturbed sand bed
12X-1	31	35	92.51	92.55	disturbed sand bed
12X-1	51	67	92.71	92.87	disturbed sandy silt
12X-2	72	82	94.42	94.52	silty clay
12X-2	86	96	94.56	94.66	silty clay
12X-2	84	85	94.54	94.55	sand bed
13X-1	60	97	98.4	98.77	silty clay
13X-2	0	75	99.02	99.77	silty clay
13X-3	0	12	100.27	100.39	silty clay
14X-1	0	70	102.8	103.5	sandy/silty clay
14X-2	0	107	104.3	105.37	sandy/silty clay
14X-2	125	150	105.55	105.8	sandy/silty clay
14X-3	0	13	105.8	105.93	sandy/silty clay
15X-1	0	8	107.4	107.48	silty clay
17X-2	60	60	123.7	123.7	silt bed
19X-2	49	70	143.19	143.4	silty clay

BSR. Specific details of the shipboard gas chemistry results for Site NGHP-01-20, Holes A and B are provided in the following discussion.

Headspace gas analyses were performed on 46 samples from NGHP-01-20A and three samples from NGHP-01-20B ranging in depth from 1.15 to 178.5 mbsf. The concentrations given here represent minimum proxy measurements of the actual concentrations due to limitations of the gas headspace method. The sediment pore water contained methane at concentrations ranging from non-detectable near the surface to 5.8 mM at 23.7 mbsf (table 6). Theoretical methane saturation in pore water under site-specific physical conditions, calculated using the Duan and others (1992), and Xu (2002, 2004) methodologies, increased from 58.9 mM at the seafloor to 131.2 mM at 190 mbsf, then decreased to 129 mM near the BSR depth of 220 mbsf. No C₂ or higher molecular weight hydrocarbon gases were detected in headspace samples, which probably indicates a microbial source of methane; however post expedition isotopic analyses will further constrain the source of gas.

Methane concentrations increase step-wise from non-detectable at 16.3 mbsf to 1.8 mM at ~17.9 mbsf, placing the SMI within this depth interval (fig. 12; see “Inorganic

Geochemistry”). Although several readings above this interval showed the presence of methane, this lower depth corresponds to other proxy indicators of the SMI (see “Inorganic Geochemistry”). Methane concentration is relatively uniform (from about 1–3 mM) from below the SMI to the borehole-completion depth of 180 mbsf. Other proxy measurements point to the presence of gas hydrate throughout this interval from 45 mbsf to 144 mbsf (see also “Inorganic Geochemistry” and “Infrared Imaging” in “Physical Properties”). The methane concentrations were generally an order of magnitude below theoretical *in-situ* saturation throughout the length of the borehole (fig. 12). However, this is probably due to preferential losses of methane during sampling and coring.

Concentrations of CO₂ ranged from 0.04 to 8.7 mM in pore water contained within the sediment (table 6). CO₂ shows a general increase with depth, though this trend is not consistent (fig. 13). CO₂ concentration is also relatively uniform (~2–4 mM) throughout the borehole depth of 180 mbsf. The methane-to-carbon dioxide ratio indicates that methane may be preferentially concentrated just below the SMI, at ~75 mbsf,

Table 4. Interstitial-water data for Hole NGHP-01-20A. The samples that were corrected for drill-water contamination are marked by bold data in the sulfate concentration column.

["-", value not determined]

Sample name	Depth (mbsf)	Vol. (mL)	pH	Alk (mM)	Salinity	Titr Cl ⁻ (mM)	Br ⁻ (mM)	SO ₄ ²⁻ (mM)	Comments
NGHP-01-20A									
1H-1 140-150	1.4	39.0	7.6	3.44	34.5	558	0.85	27.64	Brown fine clay with burrows containing coarser sediment, with some shells
1H-2 140-150	2.9	36.0	7.8	4.72	34.5	557	0.76	21.93	Brown fine clay with burrows containing coarser sediment, with some shells
1H-3 140-150	4.4	30.0	7.9	5.68	34.0	559	0.87	24.56	Brown fine clay with burrows containing coarser sediment, with some shells
1H-4 60-70	5.1	37.0	7.9	6.35	34.5	557	0.86	23.32	Brown fine clay with burrows containing coarser sediment, with some shells
2H-1 135-150	7.0	34.0	7.8	6.76	34.0	557	0.90	24.00	Brown fine clay with burrows containing coarser sediment, with some shells. Very hard for this shallow depth
2H-2 135-150	8.5	32.0	7.7	6.61	34.0	557	0.87	22.34	Brown fine clay with burrows containing coarser sediment, with some shells. Very hard for this shallow depth
2H-3 135-150	10.0	32.0	7.9	8.80	33.0	553	0.88	19.97	Brown fine clay with burrows containing coarser sediment, with some shells. Very hard for this shallow depth
2H-4 135-150	11.5	29.0	8.0	11.35	33.0	559	0.89	17.23	Brown fine clay with burrows containing coarser sediment, with some shells. Very hard for this shallow depth. Very compact, already need to cut liner in order to recover the whole round
2H-5 135-150	13.0	21.0	8.0	13.18	33.0	555	0.90	14.01	Brown fine clay with burrows containing coarser sediment, with some shells. Very hard for this shallow depth. Very compact. Liner had to be cut
2H-6 85-100	14.0	25.0	7.8	14.07	33.0	555	0.93	11.19	Had to cut liner and it was even difficult to retrieve sample from cut liner
3H-1 135-150	16.5	20.0	8.0	20.32	32.0	557	0.98	0.05	Darker sediment, brown-black. Very fine and sticky as above. A small carbonate nodule
3H-2 135-150	18.0	36.0	7.9	19.42	32.0	559	0.99	0.12	Dark, fine clay. Very sticky as above
3H-3 135-150	19.5	30.0	8.0	18.98	31.5	557	1.02	0.06	Gas expansion features observed in core and in sample. Sticky but fractured by gas
3H-4 135-150	21.0	30.0	7.9	18.14	32.0	556	1.04	0.05	Gas expansion features observed in core and in sample. Sticky but fractured by gas
3H-5 115-130	22.3	27.0	7.9	18.89	32.0	557	1.13	0.04	Dark clay and fractured
4X-1 130-150	24.2	22.0	8.0	18.56	32.0	558	1.19	0.32	Dark clay with some gas expansion features. Difficult to clean. No biscuits. Small carbonate nodule
5X-1 130-150	33.8	19.0	7.9	20.16	32.0	555	1.48	0.11	Black fine sediment. Very sticky and hard to clean. No biscuits
6X-1 135-150	43.4	20.0	7.7	19.89	31.5	550	1.43	0.92	
6X-3 36-56 HY	45.0	6.0	-	-	28.0	482	1.30	0.43	Small IR anomaly. No apparent lithologic control. Entire sample composed of fine grained material. Very difficult to clean; possible contamination with drill water
6X-3 36-56 BK	45.0	23.0	8.0	21.32	32.0	555	1.49	0.22	Fine clay with a few small carbonate nodules. Very difficult to clean.
7X-1 54-74	52.2	17.0	-	-	31.5	554	1.47	0.45	Short core. No IR anomaly. Coarse-grained and unconsolidated
9X-1 130-150	72.2	13.0	-	-	30.0	534	1.36	1.11	Short core. No IR anomaly.
10X-1 125-150	81.9	16.0	7.7	15.43	29.5	516	1.34	2.35	Short core. No IR anomaly. Extremely disturbed sample. Very wet and difficult to clean. A bit sandier. No consolidated pieces at all
11X-1 125-150	91.5	12.0	-	-	30.0	538	1.44	0.05	Again, very poor quality sample. No biscuits. A very disturbed core
12X-1 125-150	93.5	17.0	-	-	30.0	523	1.43	0.53	Again, very poor quality. No biscuits. A very disturbed core
13X-1 97-122	98.8	10.0	-	-	30.0	530	1.41	0.33	Very small IR anomaly spot in scan. No apparent anomaly in hand-held IR camera. Sediment better filled the liner than in previous cores. Very small sample
14X-1 125-150	104.1	17.0	7.9	14.72	28.5	504	1.33	0.62	A better core than 13X
15X-1 95-120	108.4	23.0	7.7	10.40	29.0	511	1.37	0.43	Only one section recovered. Poor core
16X-4 125-150 BK	118.2	26.0	7.9	13.55	29.5	514	1.38	0.22	Background sample
16X-6 21-51 HY	119.6	11.0	-	-	30.0	536	1.42	0.23	Minor double IR anomaly
16X-6 21-51 NA	119.6	24.0	7.9	14.35	30.3	547	1.46	0.24	Adjacent to anomaly
17X-1 85-110	122.9	18.0	-	-	30.0	544	1.40	0.09	Only background. Very short core. No anomalies in this core. Some carbonate
18X-1 75-100	132.4	22.0	7.3	11.84	30.0	541	1.46	0.20	Authigenic carbonate is abundant, including small nodules. An intact aragonite shell was recovered
19X-2 125-150	144.0	22.0	7.4	11.07	30.0	546	1.48	0.11	This was a highly disturbed core. Contains mini-carbonate nodules
Total depth	148.8								
NGHP-01-20B									
1X		-	-	-	-	-	-	-	Water depth 1158 m
2X		-	-	-	-	-	-	-	140.8–158.4 mbsf: Too disturbed to sample. No recovery
									158.4–168.1 mbsf: Too disturbed to sample. No recovery
3X-1 99-129	169.1	14.0	-	-	30.0	530	1.46	0.11	Very sticky and compacted. Hard to clean. Mini carbonate nodules
4X-1 89-119	178.6	9.0	-	-	29.5	517	1.41	0.19	Very sticky and compacted. Hard to clean. Mini carbonate nodules

Table 5. Interstitial-water data corrected for drill-water contamination based on sulfate concentration, for Hole NGHP-01-20A. The samples that were corrected for drill-water contamination are marked by bold data in the sulfate concentration column.

["-", value not determined]

Sample name	Depth (mbsf)	V Samp (mL)	pH	Alk (mM)	Salinity	Titr Cl ⁻ (mM)	Br ⁻ (mM)	Br ⁻ /Cl ⁻	SO ₄ ²⁻ (mM)
NGHP-01-20A									
1H-1 140-150	1.4	39.0	7.6	3.44	34.5	558	0.85	0.0015	27.64
1H-2 140-150	2.9	36.0	7.8	4.72	34.5	557	0.76	0.0014	21.93
1H-3 140-150	4.4	30.0	7.9	5.68	34.0	559	0.87	0.0016	24.56
1H-4 60-70	5.1	37.0	7.9	6.35	34.5	557	0.86	0.0016	23.32
2H-1 135-150	7.0	34.0	7.8	6.76	34.0	557	0.90	0.0016	24.00
2H-2 135-150	8.5	32.0	7.7	6.61	34.0	557	0.87	0.0016	22.34
2H-3 135-150	10.0	32.0	7.9	8.80	33.0	553	0.88	0.0016	19.97
2H-4 135-150	11.5	29.0	8.0	11.35	33.0	559	0.89	0.0016	17.23
2H-5 135-150	13.0	21.0	8.0	13.18	33.0	555	0.90	0.0016	14.01
2H-6 85-100	14.0	25.0	7.8	14.07	33.0	555	0.93	0.0017	11.19
3H-1 135-150	16.5	20.0	8.0	20.32	32.0	557	0.98	0.0018	0.05
3H-2 135-150	18.0	36.0	7.9	19.41	31.8	557	0.99	0.0018	0.00
3H-3 135-150	19.5	30.0	8.0	18.98	31.5	557	1.02	0.0018	0.06
3H-4 135-150	21.0	30.0	7.9	18.14	32.0	556	1.04	0.0019	0.05
3H-5 115-130	22.3	27.0	7.9	18.89	32.0	557	1.13	0.0020	0.04
4X-1 130-150	24.2	22.0	8.0	18.53	31.6	552	1.18	0.0021	0.00
5X-1 130-150	33.8	19.0	7.9	20.15	31.9	553	1.48	0.0027	0.00
6X-1 135-150	43.4	20.0	7.7	19.82	30.4	532	1.40	0.0026	0.00
6X-3 36-56 HY	45.0	6.0	-	-	27.5	474	1.28	0.0027	0.00
6X-3 36-56 BK	45.0	23.0	8.0	21.30	31.7	551	1.48	0.0027	0.00
7X-1 54-74	52.2	17.0	-	-	31.0	545	1.45	0.0027	0.00
9X-1 130-150	72.2	13.0	-	-	28.7	512	1.32	0.0026	0.00
10X-1 125-150	81.9	16.0	7.7	15.24	26.7	471	1.27	0.0027	0.00
11X-1 125-150	91.5	12.0	-	-	30.0	538	1.44	0.0027	0.05
12X-1 125-150	93.5	17.0	-	-	29.4	513	1.42	0.0028	0.00
13X-1 97-122	98.8	10.0	-	-	29.6	524	1.40	0.0027	0.00
14X-1 125-150	104.1	17.0	7.9	14.67	27.7	492	1.31	0.0027	0.00
15X-1 95-120	108.4	23.0	7.7	10.37	28.5	503	1.35	0.0027	0.00
16X-4 125-150 BK	118.2	26.0	7.9	13.53	29.2	510	1.37	0.0027	0.00
16X-6 21-51 HY	119.6	11.0	-	-	29.7	531	1.42	0.0027	0.00
16X-6 21-51 NA	119.6	24.0	7.9	14.33	30.0	542	1.45	0.0027	0.00
17X-1 85-110	122.9	18.0	-	-	30.0	544	1.40	0.0026	0.09
18X-1 75-100	132.4	22.0	7.3	11.82	29.8	537	1.45	0.0027	0.00
19X-2 125-150	144.0	23.0	7.4	11.06	29.9	544	1.48	0.0027	0.00
NGHP-01-20B									
1X	-	-	-	-	-	-	-	-	-
2X	-	-	-	-	-	-	-	-	-
3X-1 99-129	169.1	14.0	-	-	29.9	528	1.46	0.0028	0.00
4X-1 89-119	178.6	9.0	-	-	29.3	513	1.41	0.0027	0.00

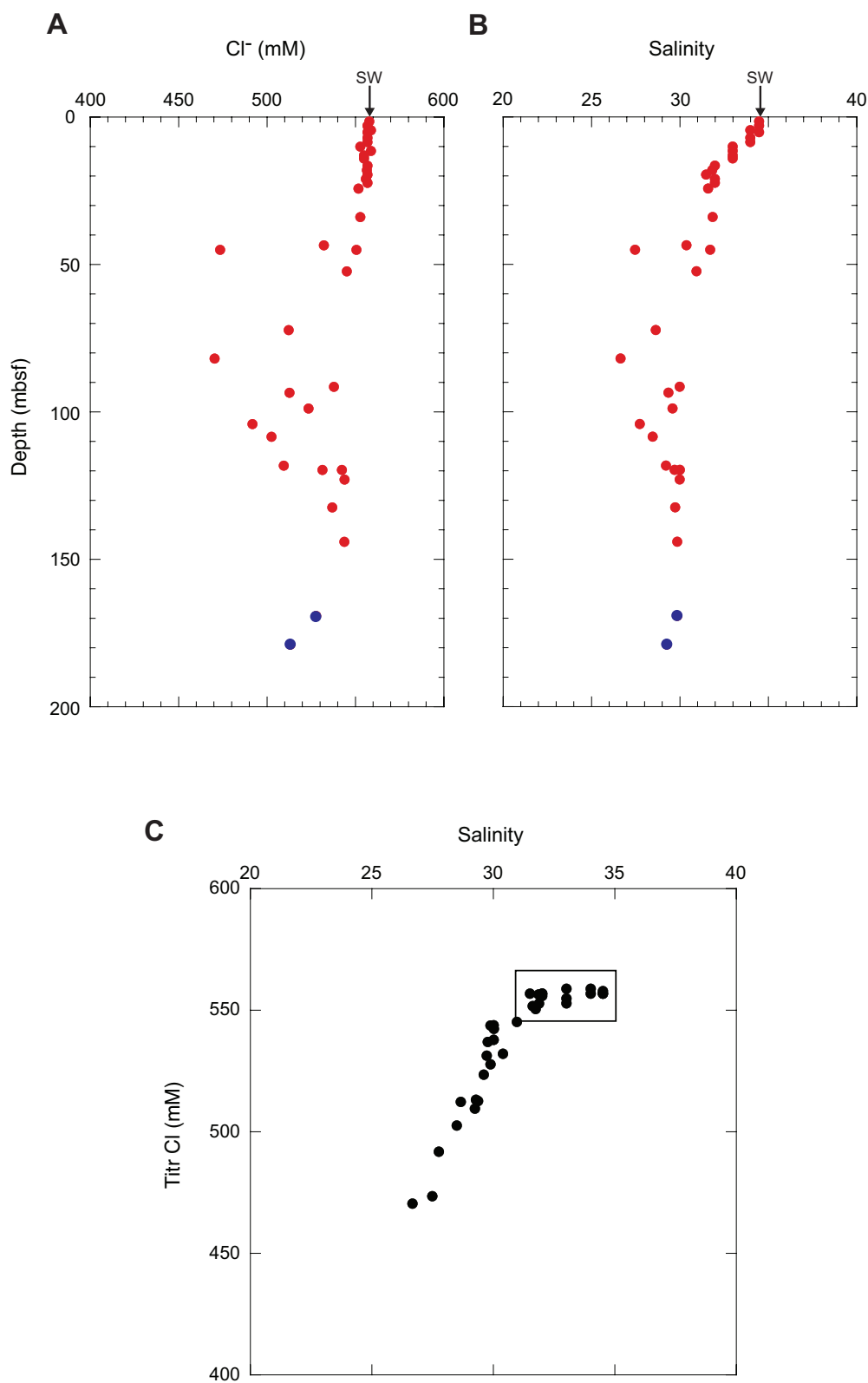


Figure 9. Concentration-depth profiles of A, chloride and B, salinity at Hole NGHP-01-20A. C, Cross plot between dissolved chloride concentration and salinity, showing a good correspondence for samples deeper than 40 mbsf, where both parameters are primarily influenced by dilution of the fluids by hydrate dissociation. Shallower samples, where salinity is modified by diagenetic reactions and chloride is not, are demarcated by a box. Seawater value is designated as "sw" in A and B. [mbsf, meters below sea floor]

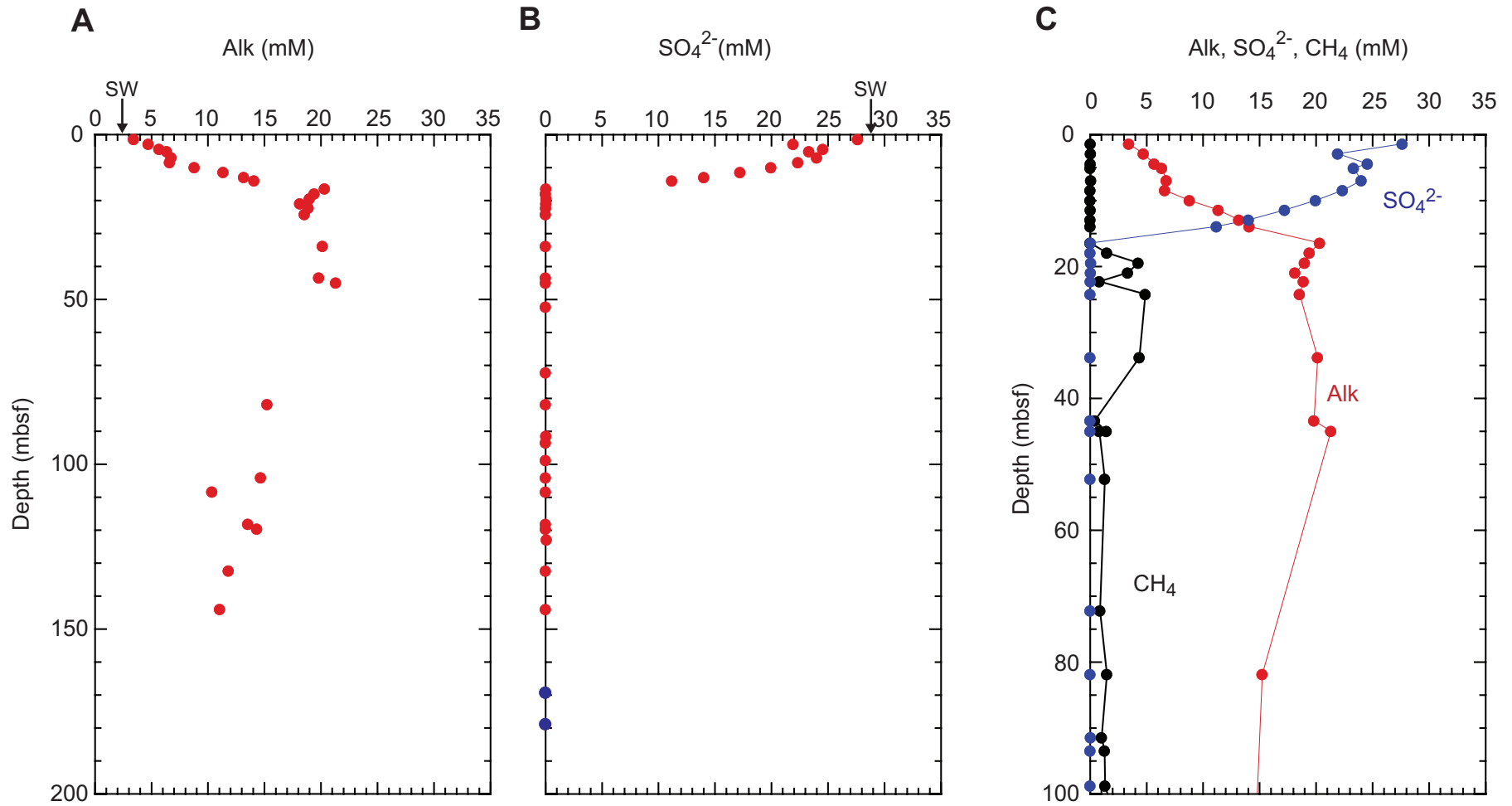


Figure 10. A, Concentration-depth profiles of alkalinity; B, sulfate; and C, sulfate, methane, and alkalinity at Hole NGHP-01-20A. Note the alkalinity maximum at the SMI depth (21 mbsf) and the steep increase in methane concentration below the SMI. Seawater value is designated as "sw" in A and B. [SMI, sulfate-methane interface; mbsf, meters below sea floor]

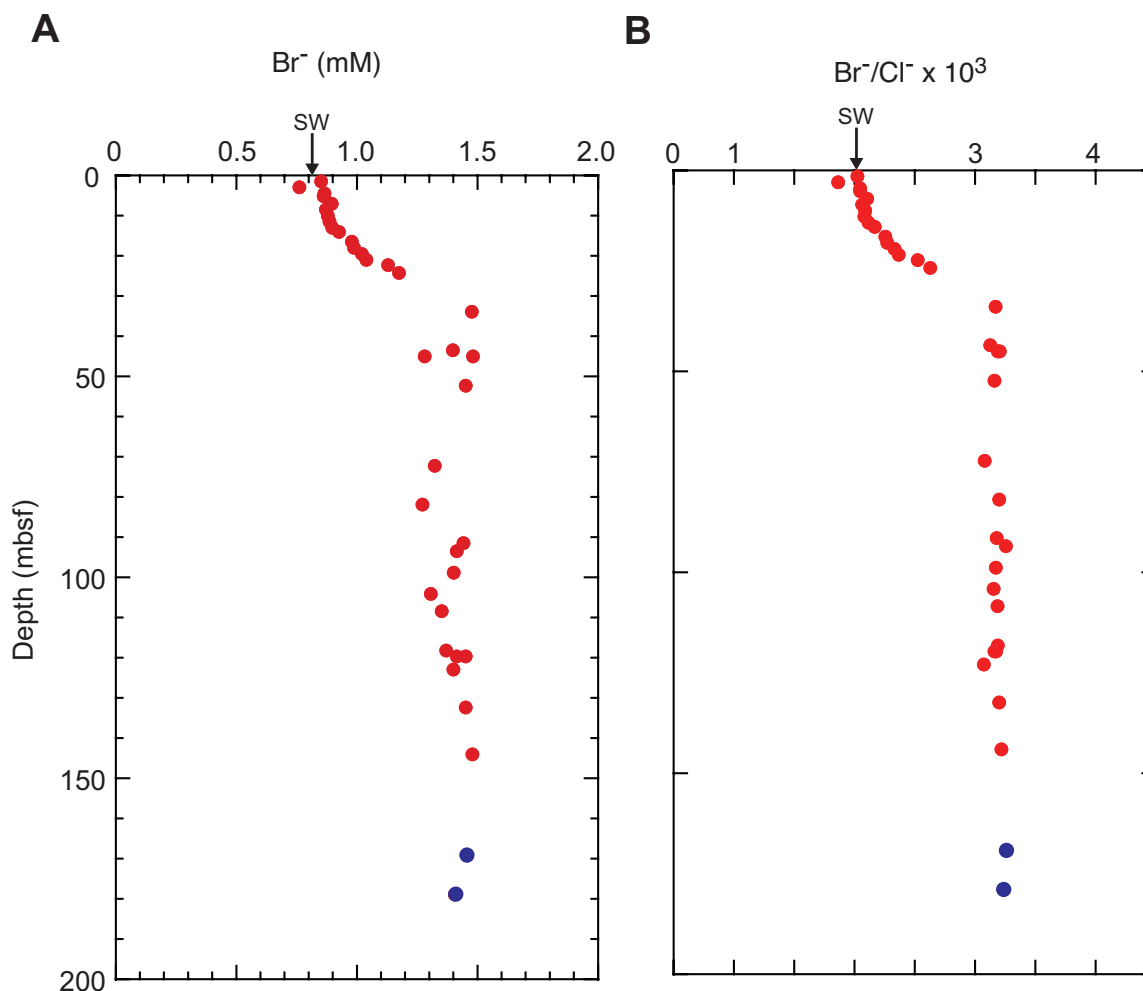


Figure 11. Concentration-depth profile of dissolved bromide at Hole NGHP-01-20A. Seawater value is designated as “sw.”

and again near 135 mbsf (fig. 14). These intervals occur within the zone of predicted gas hydrate but not where Cl^- anomalies showed the highest concentration of gas hydrate at 45 and 80 mbsf (see “Inorganic Geochemistry”). Some portion of the variability observed for samples in this borehole may be due to preferential loss of methane in headspace sampling and/or XCB coring agitation, which started at 23.7 mbsf. The air gases (N_2+Ar) and O_2 were the balance gases. However, the (N_2+Ar)/ O_2 ratios were typically $>$ air reflecting the ratios in the sediment—these ratios may also indicate that some air was trapped in the headspace samples and that some oxygen has likely dissolved preferentially compared to N_2 . Air gases are present in all samples as the core plugs were degassed in an air headspace. No free gas or void gas samples were collected and no pressure core degassing experiments were completed at Site NGHP-01-20.

Microbiology

Hole NGHP-01-20A

Analysis of all microbiological samples will be shore-based. Twenty-two samples were collected for shore-based analysis of lipid content, gene characterization and fluorescent *in-situ* hybridization (table 7). Additional microbiological samples were taken under the following sample codes: MAF, MAG, MAR, MBF, MBG, and MBR. Fourteen microbiological samples were also taken under Lab code JUD, and fourteen samples under lab code JAN.

Hole NGHP-01-20B

No microbiological samples were collected for this hole.

Table 6. Headspace gas composition for Site NGHP-01-20.

Sample	Site	Hole	Core	Section	Interval (cm)	Sed wt. (g)	Sample depth (mbsf)	CO ₂ (ppmv)	C ₁	C ₂
20A-1H1-115-120	20	A	1	1	115-120	14.5	1.15	16,900	500	nd
20A-1H2-135-140	20	A	1	2	135-140	8.4	2.85	15,500	300	nd
20A-1H3-90-95	20	A	1	3	90-95	10.7	3.90	18,800	200	nd
20A-1H4-55-60	20	A	1	4	55-60	13.8	5.05	4,100	nd	nd
20A-2H1-120-125	20	A	2	1	120-125	9.6	6.80	2,600	400	nd
20A-2H2-130-135	20	A	2	2	130-135	7.0	8.40	11,400	nd	nd
20A-2H3-110-115	20	A	2	3	110-115	11.4	9.70	12,300	100	nd
20A-2H4-130-135	20	A	2	4	130-135	11.6	11.40	24,900	300	nd
20A-2H5-85-90	20	A	2	5	85-90	12.5	12.45	48,500	nd	nd
20A-2H6-80-85	20	A	2	6	80-85	9.8	13.90	1,400	nd	nd
20A-3H1-120-125	20	A	3	1	120-125	12.5	16.30	400	nd	nd
20A-3H2-130-135	20	A	3	2	130-135	12.4	17.90	9,800	14,500	nd
20A-3H3-110-115	20	A	3	3	110-115	10.4	19.20	52,800	31,400	nd
20A-3H4-85-90	20	A	3	4	85-90	13.3	20.45	16,800	35,600	nd
20A-3H5-110-115	20	A	3	5	110-115	12.6	22.20	12,300	7,900	nd
20A-4X1-75-80	20	A	4	1	75-80	9.5	23.65	13,100	30,900	nd
20A-4X1-80-85	20	A	4	1	80-85	10.9	23.70	11,500	33,700	nd
20A-5X1-75-80	20	A	5	1	75-80	9.5	33.25	5,400	2,400	nd
20A-5X1-80-85	20	A	5	1	80-85	9.1	33.30	7,900	8,300	nd
20A-6X1-75-80	20	A	6	1	75-80	9.6	42.85	12,400	5,000	nd
20A-6X1-80-85	20	A	6	1	80-85	8.4	42.90	10,900	6,700	nd
20A-6X3-31-36	20	A	6	3	31-36	8.7	44.91	10,900	4,600	nd
20A-7X1-49-54	20	A	7	1	49-54	9.4	52.19	17,500	8,700	nd
20A-9X1-75-80	20	A	9	1	75-80	9.7	71.65	2,700	6,000	nd
20A-9X1-80-85	20	A	9	1	80-85	9.4	71.70	8,300	7,300	nd
20A-10X1-70-75	20	A	10	1	70-75	11.4	81.30	9,200	9,700	nd
20A-10X1-75-80	20	A	10	1	75-80	7.6	81.35	7,200	9,800	nd
20A-11X1-95-100	20	A	11	1	95-100	10.6	91.15	9,100	2,700	nd
20A-11X1-100-105	20	A	11	1	100-105	9.4	91.20	9,700	9,300	nd
20A-12X1-75-80	20	A	12	1	75-80	11.3	92.95	16,100	6,000	nd
20A-13X1-92-97	20	A	13	1	92-97	9.7	98.72	13,100	5,600	nd
20A-13X2-70-75	20	A	13	2	70-75	9.1	99.72	12,200	8,200	nd
20A-13X2-75-80	20	A	13	2	75-80	12.4	99.77	13,600	11,700	nd
20A-14X1-75-80	20	A	14	1	75-80	12.6	103.50	28,300	15,600	nd
20A-14X1-70-75	20	A	14	1	70-75	11.5	103.55	17,900	8,200	nd
20A-15X1-70-75	20	A	15	1	70-75	9.1	108.05	27,400	15,800	nd
20A-15X1-65-70	20	A	15	1	65-70	10.8	108.10	40,000	14,200	nd
20A-16X4-70-75	20	A	16	4	70-75	12.0	117.60	11,600	4,500	nd
20A-16X4-75-80	20	A	16	4	75-80	12.0	117.65	52,100	14,100	nd
20A-16X6-16-21	20	A	16	6	16-21	10.2	119.56	20,700	11,100	nd
20A-17X1-30-35	20	A	17	1	30-35	11.6	122.30	28,700	7,800	nd
20A-17X1-35-40	20	A	17	1	35-40	11.8	122.35	38,100	18,900	nd
20A-18X1-45-50	20	A	18	1	45-50	10.1	132.05	900	2,300	nd
20A-18X1-50-55	20	A	18	1	50-55	10.8	132.10	4,600	14,500	nd
20A-19X2-70-75	20	A	19	2	70-75	10.0	143.40	6,000	7,900	nd
20A-19X2-75-80	20	A	19	2	75-80	7.2	143.45	20,100	7,800	nd
20B-1X1-37-42	20	B	1	1	37-42	9.3	149.17	9,600	5,800	nd
20B-3X1-94-99	20	B	3	1	94-99	9.1	169.04	9,900	8,600	nd
20B-4X1-84-89	20	B	4	1	84-89	9.7	178.54	20,100	9,700	nd

Table 6. Headspace gas composition for Site NGHP-01-20.—Continued

Sample	C ₃	O ₂	N ₂ +Ar	H ₂ S	C ₁ (μL/L WS)	C ₁ (mM PW)	CO ₂ (μL/L WS)	CO ₂ (mM PW)	C ₁ /CO ₂
20A-1H1-115-120	nd	174,800	754,100	nd	600	0.0	19,800	1.1	0.0
20A-1H2-135-140	nd	184,100	744,100	nd	900	0.1	42,500	2.7	0.0
20A-1H3-90-95	nd	172,700	743,600	nd	300	0.0	36,600	2.4	0.0
20A-1H4-55-60	nd	182,800	756,100	nd	nd	nd	5,200	0.4	-
20A-2H1-120-125	nd	191,200	747,000	nd	1,000	0.1	6,000	0.4	0.2
20A-2H2-130-135	nd	188,900	763,200	nd	nd	nd	39,800	2.8	-
20A-2H3-110-115	nd	176,400	724,700	nd	200	0.0	21,700	1.6	0.0
20A-2H4-130-135	nd	172,600	753,000	nd	500	0.0	42,700	3.2	0.0
20A-2H5-85-90	nd	171,500	751,600	nd	nd	nd	73,800	5.7	-
20A-2H6-80-85	nd	195,400	741,800	nd	nd	nd	3,100	0.2	-
20A-3H1-120-125	nd	197,100	744,000	nd	nd	nd	600	0.0	-
20A-3H2-130-135	nd	177,100	715,100	nd	22,300	1.8	15,000	1.2	1.5
20A-3H3-110-115	nd	146,500	725,700	nd	63,700	5.1	107,100	8.6	0.6
20A-3H4-85-90	nd	141,700	727,300	nd	48,700	4.0	23,000	1.9	2.1
20A-3H5-110-115	nd	165,800	742,600	nd	11,900	1.0	18,500	1.5	0.6
20A-4X1-75-80	nd	177,400	755,200	nd	71,600	5.8	30,200	2.5	2.4
20A-4X1-80-85	nd	158,600	773,800	nd	63,700	5.2	21,800	1.8	2.9
20A-5X1-75-80	nd	195,100	763,500	nd	5,600	0.5	12,500	1.1	0.4
20A-5X1-80-85	nd	175,300	788,800	nd	20,300	1.7	19,500	1.7	1.1
20A-6X1-75-80	nd	167,700	787,900	nd	11,300	1.0	28,400	2.5	0.4
20A-6X1-80-85	nd	178,600	762,700	nd	18,300	1.6	30,000	2.6	0.6
20A-6X3-31-36	nd	186,100	766,600	nd	12,100	1.1	28,500	2.5	0.4
20A-7X1-49-54	nd	169,900	778,300	nd	20,500	1.8	41,200	3.7	0.5
20A-9X1-75-80	nd	180,100	762,400	nd	13,600	1.3	6,100	0.6	2.2
20A-9X1-80-85	nd	180,400	784,900	nd	17,000	1.6	19,600	1.8	0.9
20A-10X1-70-75	nd	132,900	834,000	nd	17,200	1.7	16,300	1.6	1.1
20A-10X1-75-80	nd	168,500	781,000	nd	30,900	2.9	22,500	2.1	1.4
20A-11X1-95-100	nd	171,400	750,300	nd	5,300	0.5	17,900	1.7	0.3
20A-11X1-100-105	nd	116,900	833,500	nd	21,800	2.1	22,800	2.2	1.0
20A-12X1-75-80	nd	118,200	820,600	nd	10,800	1.1	28,700	2.8	0.4
20A-13X1-92-97	nd	155,100	802,500	nd	12,600	1.2	29,400	2.9	0.4
20A-13X2-70-75	nd	137,700	807,000	nd	20,300	2.0	30,000	2.9	0.7
20A-13X2-75-80	nd	74,000	858,300	nd	17,900	1.8	20,900	2.1	0.9
20A-14X1-75-80	nd	161,400	789,700	nd	23,400	2.4	42,400	4.3	0.6
20A-14X1-70-75	nd	164,700	773,400	nd	14,300	1.4	31,100	3.1	0.5
20A-15X1-70-75	nd	150,600	789,200	nd	39,000	3.8	67,500	6.6	0.6
20A-15X1-65-70	nd	86,600	807,700	nd	27,200	2.7	76,600	7.6	0.4
20A-16X4-70-75	nd	127,300	786,000	nd	7,200	0.7	18,800	1.9	0.4
20A-16X4-75-80	nd	46,800	868,900	nd	22,800	2.3	84,600	8.6	0.3
20A-16X6-16-21	nd	98,000	811,800	nd	23,200	2.3	43,200	4.3	0.5
20A-17X1-30-35	nd	81,600	838,200	nd	13,300	1.4	49,200	5.0	0.3
20A-17X1-35-40	nd	102,400	833,800	nd	31,500	3.2	63,700	6.5	0.5
20A-18X1-45-50	nd	191,500	747,600	nd	4,900	0.5	1,900	0.2	2.6
20A-18X1-50-55	nd	163,800	771,000	nd	27,800	2.8	8,800	0.9	3.2
20A-19X2-70-75	nd	151,300	765,200	nd	17,000	1.7	12,800	1.3	1.3
20A-19X2-75-80	nd	138,400	836,700	nd	26,400	2.6	67,900	6.8	0.4
20B-1X1-37-42	nd	181,700	779,200	nd	13,800	1.4	22,800	2.3	0.6
20B-3X1-94-99	nd	147,500	787,300	nd	21,100	2.2	24,300	2.5	0.9
20B-4X1-84-89	nd	145,400	799,800	nd	21,700	2.3	45,100	4.7	0.5

Notes: nd = not detected. WS = Wet sediment. PW = porewater. Approximate detection limits are about 15 ppmv for methane, 30 ppmv for ethane, 50 ppmv for propane, and 20 ppmv for hydrogen sulfide.

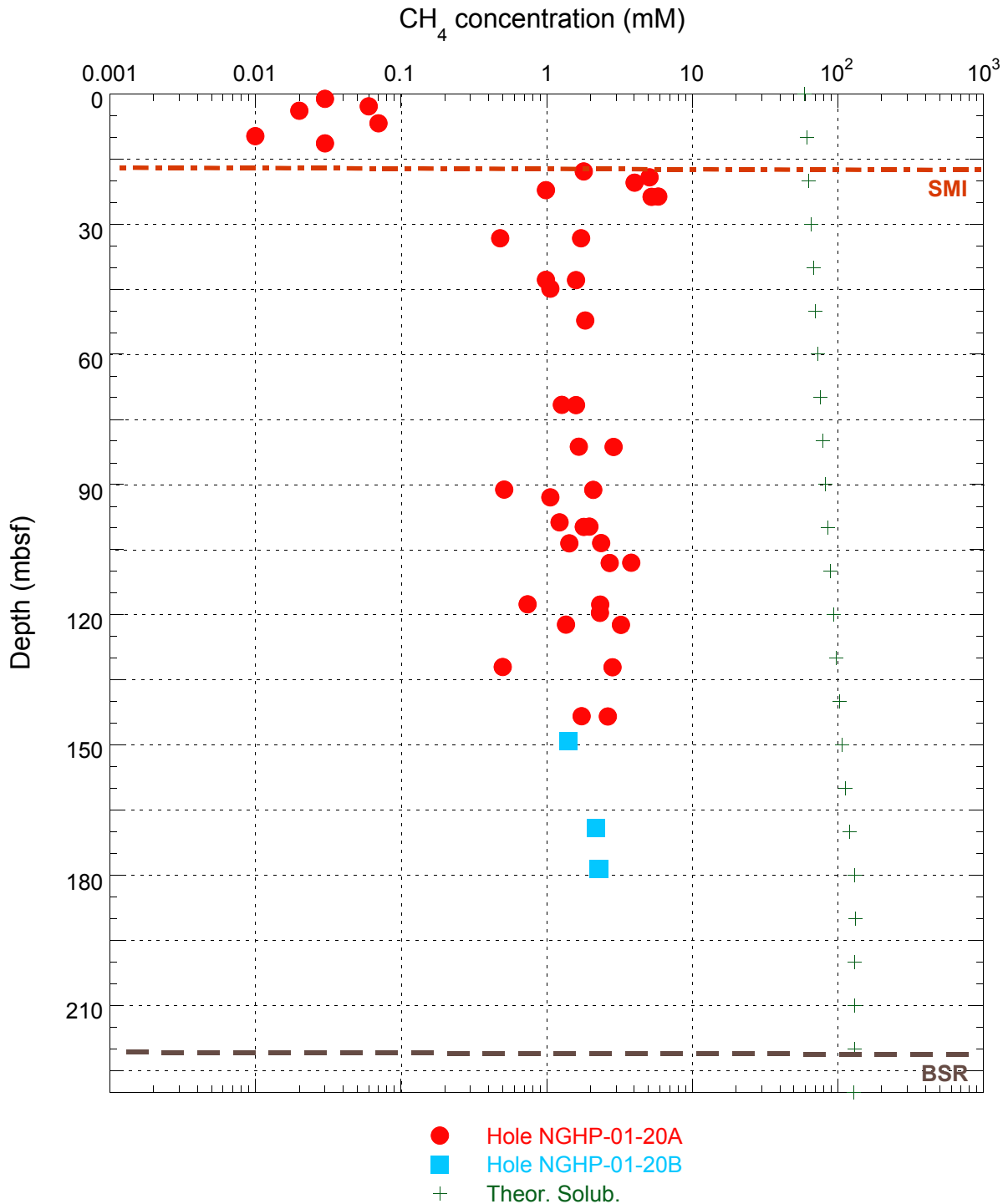


Figure 12. Plot of headspace methane gas concentration (mM) with depth for Hole NGHP-01-20A. Note the methane gradient just below 17 mbsf, indicating that the SMI occurs in this interval, despite very low methane concentrations above. Values less than 0.003 mM are below instrument detection limits but plotted for reference. Theoretical solubility of methane calculated using the Duan and others, (2002) and Xu (2002, 2004) methodologies. [mbsf, meters below sea floor; SMI, sulfate-methane interface]

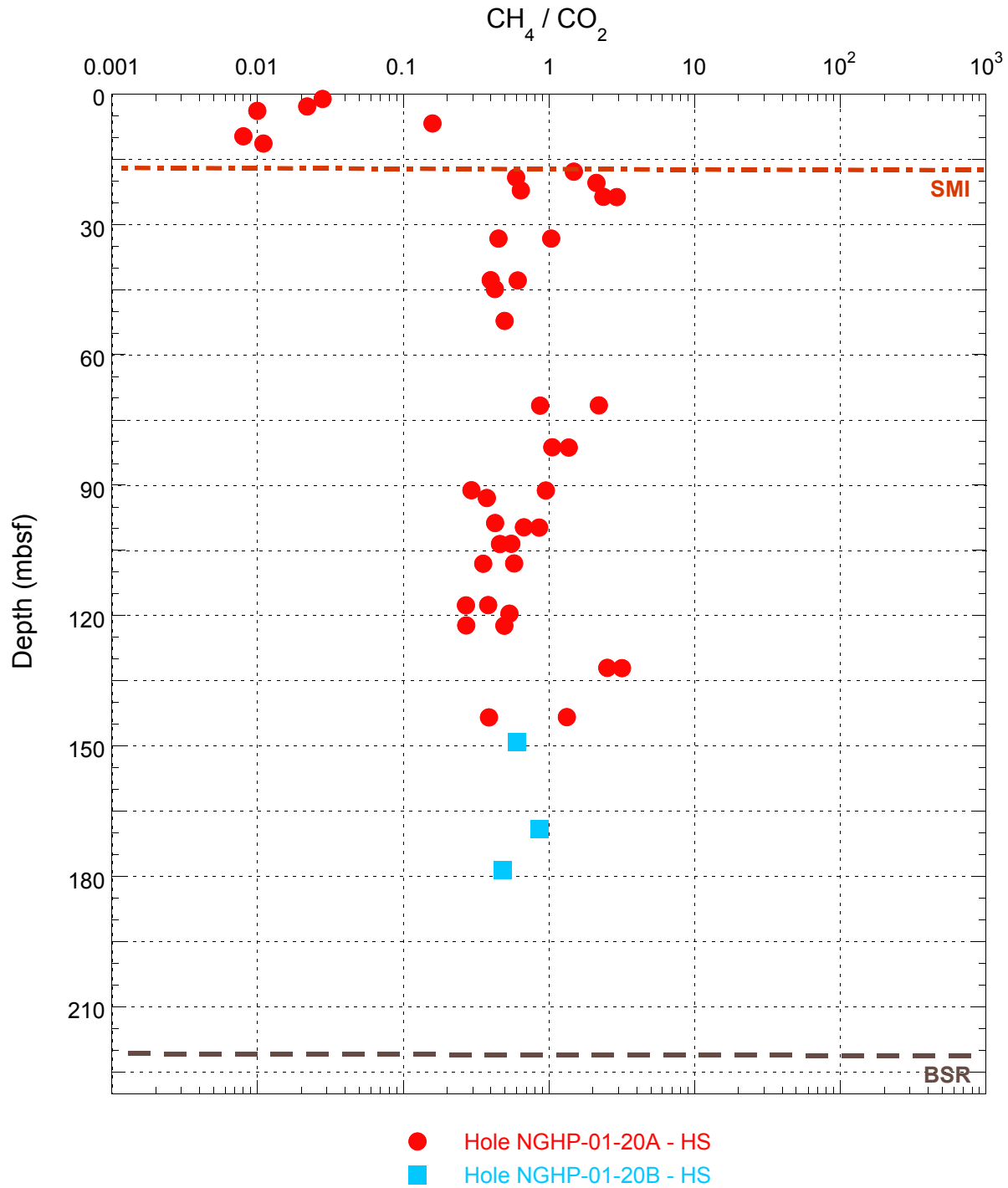


Figure 14. Plot of methane to carbon dioxide gas ratio with depth for headspace, void gas, and PCS gas for Hole NGHP-01-20A. Note the minor peaks in methane concentration, perhaps indicating the presence of free gas or gas hydrate. Preferential losses of methane during core handling and by sample procedures may result in decreases in ratio magnitude. [PCS, pressure core sampler]

Table 7. List of microbiological samples taken for Site NGHP-01-20.

Core, section	Sample code	Sample reference		Depth (mbsf)	Volume (cc)	Comments
		Top (cm)	Bottom (cm)			
NGHP-01-20A						
1H-3	JAN	105	110	4.05	187	
2H-5	JAN	100	105	12.6	187	
3H-4	JAN	100	105	20.6	187	
4X-1	JAN	95	100	23.85	187	
5X-1	JAN	95	100	33.45	187	
6X-1	JAN	95	100	43.05	187	
9X-1	JAN	95	100	71.85	187	
10X-1	JAN	90	95	81.5	187	
12X-1	JAN	90	95	93.1	187	
13X-2	JAN	90	95	99.92	187	
14X-1	JAN	90	95	103.7	187	
16X-4	JAN	90	95	117.8	187	
17X-1	JAN	50	55	122.5	187	
19X-2	JAN	90	95	143.6	187	
1H-3	JUD	120	130	4.2	374	
2H-5	JUD	115	125	12.75	374	
3H-4	JUD	115	125	20.75	374	
4X-1	JUD	110	120	24	374	
5X-1	JUD	110	120	33.6	374	
6X-1	JUD	110	120	43.2	374	
9X-1	JUD	110	120	72	374	
10X-1	JUD	105	115	81.65	374	
12X-1	JUD	105	115	93.25	374	
13X-2	JUD	105	115	100.07	374	
14X-1	JUD	105	115	103.85	374	
16X-4	JUD	105	115	117.95	374	
17X-1	JUD	65	75	122.65	374	
19X-2	JUD	105	115	143.75	374	
1H-1	LIP	120	130	1.2	374	
1H-3	LIP	95	105	3.95	374	
2H-1	LIP	125	135	6.85	5	
2H-3	LIP	115	125	9.75	374	
2H-5	LIP	90	100	12.5	374	
3H-1	LIP	125	135	16.35	374	
3H-3	LIP	115	125	19.25	374	
3H-4	LIP	90	100	20.5	374	
4X-1	LIP	85	95	23.75	374	
5X-1	LIP	85	95	33.35	374	
6X-1	LIP	85	95	42.95	374	
9X-1	LIP	85	95	71.75	374	
10X-1	LIP	80	90	81.4	374	
11X-1	LIP	105	115	91.25	374	
12X-1	LIP	80	90	93	374	
13X-2	LIP	80	90	99.82	374	
14X-1	LIP	80	90	103.6	374	
15X-1	LIP	75	85	108.15	374	
16X-4	LIP	80	90	117.7	374	
17X-1	LIP	40	50	122.4	374	
18X-1	LIP	55	65	132.15	374	
19X-2	LIP	80	90	143.5	374	
16X-7	MAF	75	80	120.66	187	MBIO ANOMALY FREEZER
16X-7	MAG	80	85	120.71	187	MBIO ANOMALY GRAINSIZE
16X-7	MAR	70	75	120.61	187	MBIO ANOMALY REEFER (DEPTH 815 CM)
16X-2	MBF	140	145	115.3	187	MBIO BKG FREEZER
16X-2	MBG	145	150	115.35	187	MBIO BKG GRAINSIZE
16X-2	MBR	135	140	115.25	187	MBIO BKG REEFER (DEPTH 280 CM)

Physical Properties

Whole-round cores at NGHP Expedition 01, Site 20 were imaged using an IR camera on the catwalk to determine the location of temperature anomalies on the surface of core liners and to enable sections containing potential gas hydrate to be quickly removed, preserved, and studied. After IR imaging was finished, non-destructive measurements were conducted on temperature-equilibrated, whole-round core sections with the MSCL. Thermal conductivity measurements were also conducted on whole-round cores. Various tests were performed on split cores including: electrical resistivity by use of a Wenner array, *P*-wave velocity by inserted spades, and shear strength by mini-vane and Pocket Penetrometer. Core subsamples were placed in 10-mL beakers and dried at 105 °C for at least 24 hr to determine water content. Subsequently, the dried samples were analyzed for grain density using gas pycnometers and other sediment parameters were then calculated. See the “Physical Properties” section of the “Methods” chapter for more details.

The physical properties program at Site NGHP-01-20 focused on Holes NGHP-01-20A and NGHP-01-20B drilled in the KG Basin (~40 km off the east coast of India) in about 1,146 m of water. Site NGHP-01-20 is about 3.5 km SSE of Site NGHP-01-10, a location that yielded significant amounts of gas hydrate earlier during NGHP-01. Hole NGHP-01-20A was continuously cored to 147.8 mbsf but produced very poor recovery (46.5 percent) of core. Hole NGHP-01-20B was washed down to 148.8 mbsf and coring was re-attempted, however, with even worse recovery (9.5 percent). Hole NGHP-01-20B was abandoned at a depth of 187.3 m. IR images indicated that gas hydrates may have been present in disseminated form from ~45 to 144 mbsf.

Infrared Imaging

Environmental Conditions

The catwalk environment was monitored during the entire drilling operation at Site NGHP-01-20 (Holes NGHP-01-20A and NGHP-01-20B). Temperature on the catwalk averaged ~29 °C, ranging from 25.5 to 30.5 °C during drilling operations, with one significant and relatively rapid temperature drop associated with a heavy rainstorm (fig. 15). Relative humidity ranged from 75 to 96 percent (fig. 15), which is consistent with the marine environmental setting of the north-western Bay of Bengal. Other than temperature and relatively humidity transients, adverse environmental conditions were not present during drilling operations at this site.

Near-surface seawater temperature was measured at this using a temperature logger deployed over the port side midship. Seawater temperature was relatively constant at 28 °C.

Infrared Images

All APC and XCB cores from Site NGHP-01-20, Hole A, were systematically scanned upon arrival on the catwalk using the track-mounted IR camera described in the “Physical Properties” section of the “Methods” chapter. IR anomalies, commonly referred to as “cold spots,” indicate gas-hydrate dissociation during core recovery, which provided guidance to catwalk sampling. Summary digital maps of the scans of all cores are available on the data DVD that accompanies this report and listings of the image files are presented in tables 8 and 9. Temperature arrays in text-formatted files were exported from the IR camera software and then concatenated for each core. The arrays were then further concatenated for all cores available in a given borehole. Downcore temperatures were averaged for each pixel row in the array, excluding pixels ~1 cm from the edge of the image and <2 cm from the midline of the image. Exclusion of these pixels minimized the effects caused by major thermal artifacts in the images. This processing enabled us to measure the average amplitude of the cold anomalies and identify warm anomalies due to voids from the background temperature field.

IR track imaging at Site NGHP-01-20A consisted of 22 scans for a total scanned core length of ~80 m. The complete set of IR images collected for borehole NGHP-01-20A is presented in figure 16 along with the corresponding downcore temperatures. The core liner surface temperature extracted from the IR images for Hole NGHP-01-20A ranged from a high of ~27 °C on void sections of the core liner throughout the hole to a low of ~17 °C at an IR anomaly at ~45 mbsf. Spikes at the end of cores were as high as 30 °C. In contrast with many other NGHP Expedition 01 sites, core liners near the top of the borehole are only slightly cooler than deeper cores. The first IR anomaly attributable to gas hydrate occurs at a relatively shallow depth in core 6X (~45 mbsf). Other distinct cool zones in the core occur between ~104 and 144 mbsf and are shown by red arrows on figure 16. There is also a zone between 104 and 135 mbsf where cores are generally cooler, especially Cores NGHP-01-20A-16X and NGHP-01-20A-17X, suggesting that there may be a background of disseminated hydrate in addition to more localized gas hydrate that is responsible for the discrete IR anomalies. The IR anomalies are confirmed by a decrease in chlorinity (see “Inorganic Geochemistry”). The overall occurrence of cooler cores between 104 and 135 mbsf was compared to core-end images. Figure 17 shows two such images and their quantitative cross-core temperature profiles, one in Core NGHP-01-20A-10X and the other in Core NGHP-01-20A-16X. The image from NGHP-01-20A-16X is cooler than the one from NGHP-01-20A-10X, supporting the hypothesis that disseminated hydrate may be present in the vicinity of 104 to 135 mbsf. However, all conclusions about the location of gas hydrate at this site are limited by poor core recovery in both Holes NGHP-01-20A and NGHP-01-20B.

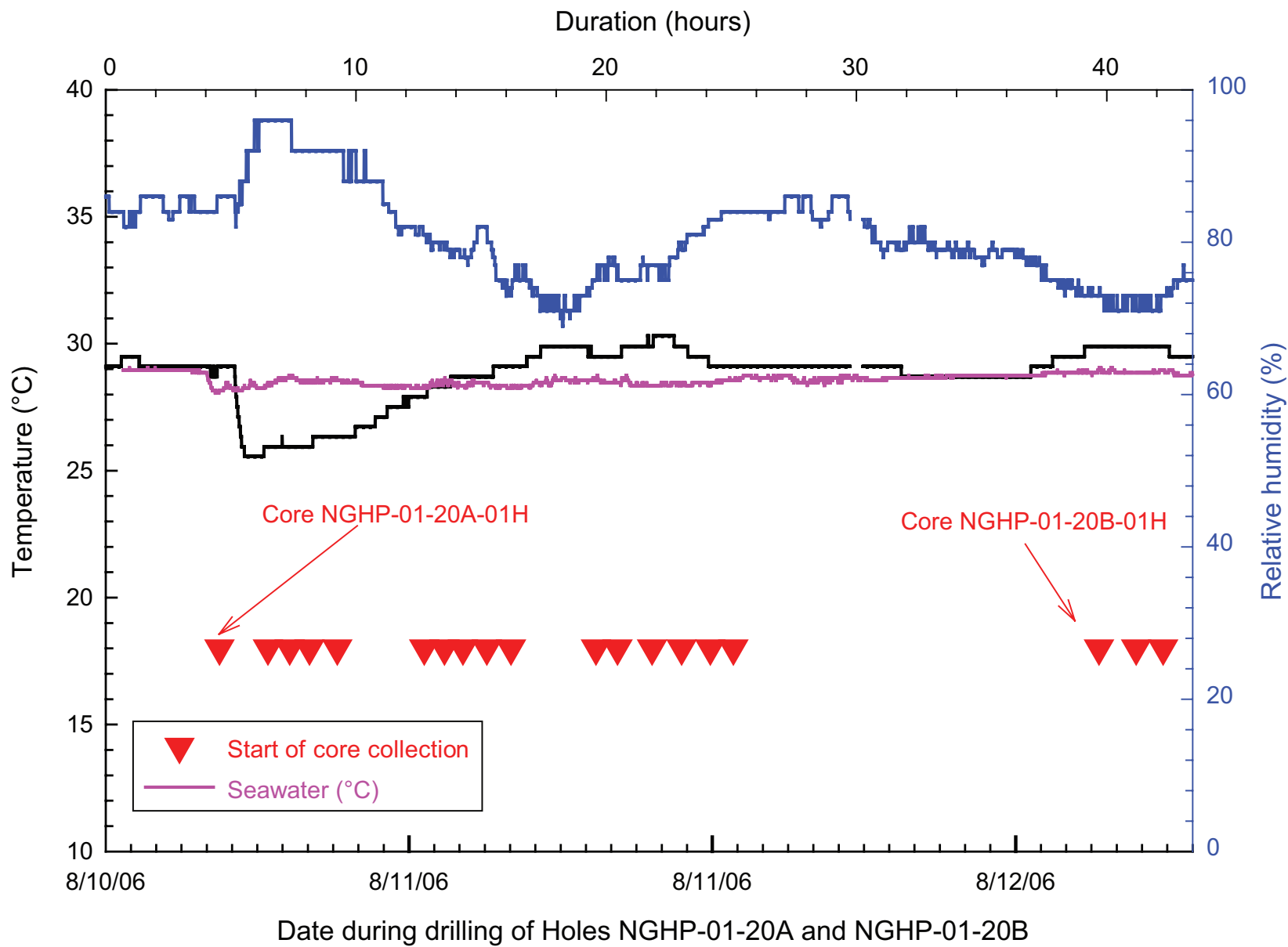


Figure 15. Catwalk temperature and humidity measurements as a function of time during drilling operations at Site NGHP-01-20.

Table 8. List of infrared images collected from Hole NGHP-01-20A.

Site:	NGHP-01-20		NGHP Expedition 01			
Hole:	A		Infrared thermal imaging track			
Core	Imaging length (cm)	First run	Date	Start time	Temperature (start/end) (°C)	Comments
1H	205	x	8/10	19:33	29.5/29.5	Short, hit mudline but hole abandoned
1HA	535		8/10	20:04	29.1/29.1	Good mudline, actual 1H for hole
2H	925	x	8/10	21:13	29.1/29.1	
3H	740	x	8/10	22:30	29.1/29.1	Stiff core, not a full barrel
4X	190	x	8/11	0:25	25.5/25.5	
5X	240	x	8/11	1:17	25.9/25.9	
6X	340	x	8/11	2:04	25.9/25.9	Small IR anomaly @~295 cm
7X	90	x	8/11	3:10	26.3/26.3	
8X						No scan, Core too short.
9X	170	x	8/11	6:36	27.9/27.9	
10X	180	x	8/11	7:24	28.3/28.3	
11X	190	x	8/11	8:08	28.7/28.7	
12X	260	x	8/11	9:05	28.7/28.7	
13X	280	x	8/11	10:02	29.1/29.1	
14X	380	x	8/11	13:24	29.9/29.9	
15X	145	x	8/11	14:15	29.5/29.5	
16X	945	x	8/11	15:37	29.9/29.9	
17X	350	x	8/11	16:47	30.3/30.3	
18X	265	x	8/11	17:55	29.5/29.5	
19X	340	x	8/11	18:50	29.5/29.5	
1X	60	x	8/12	9:18	29.9/29.9	
2X						No scan. No core.
3X	140	x	8/12	10:46	29.9/29.9	
4X	950	x	8/12	11:50	29.9/29.9	

Table 9. List of infrared image files collected from section ends from Hole NGHP-01-20A.

Core	Section	Top	Bottom	Date	Time	Image #	Comments
1H				8/10			
1Ha	2		x	8/10	20:15	G0810-01, 02	IMG file odd numbers, BMP even #'s
2H	2		x	8/10	21:27	G0810-03, 04	
3H	3		x	8/10	22:43	G0810-05, 06	
4X	2	x		8/11	0:35	G0811-01, 02	
5X	2	x		8/11	1:25	G0811-03, 04	
6X	3		x	8/11	2:07	G0811-05, 06	Image above IW sample (anomaly at 36 cm)
7X	1	x		8/11	3:12	G0811-07, 08	
8X	1	x		8/11	3:59	G0811-09, 10	10 cm section
9X	2	x		8/11	6:45	G0811-11, 12	
10X	2	x		8/11	7:27	G0811-13, 14	
11X	2	x		8/11	8:15	G0811-15, 16	
12X	2	x		8/11	9:12	G0811-17, 18	
13X	3	x		8/11	10:18	G0811-19, 20	
14X	2	x		8/11	13:31	G0811-21, 22	2 cm below 3 m mark on catawalk scan
15X							No image, core end fractured, broken
16X	3		x	8/11	15:52	G0811-23, 24	
16X	3	x		8/11	15:52	G0811-25, 26	
17X	3	x		8/11	16:55	G0811-27, 28	
18X	3	x		8/11	18:02	G0811-29, 30	
19X	1		x	8/11	18:57	G0811-31, 32	Rough surface, gashes (similar in most)
1X							No core ends available
2X							No core ends available
3X	1		x	8/12	11:53	G0812-01, 02	Bottom of section 1 at 129 cm (just above IW)
4X	1		x	8/12	11:56	G0812-03, 04	At 84 cm above IW

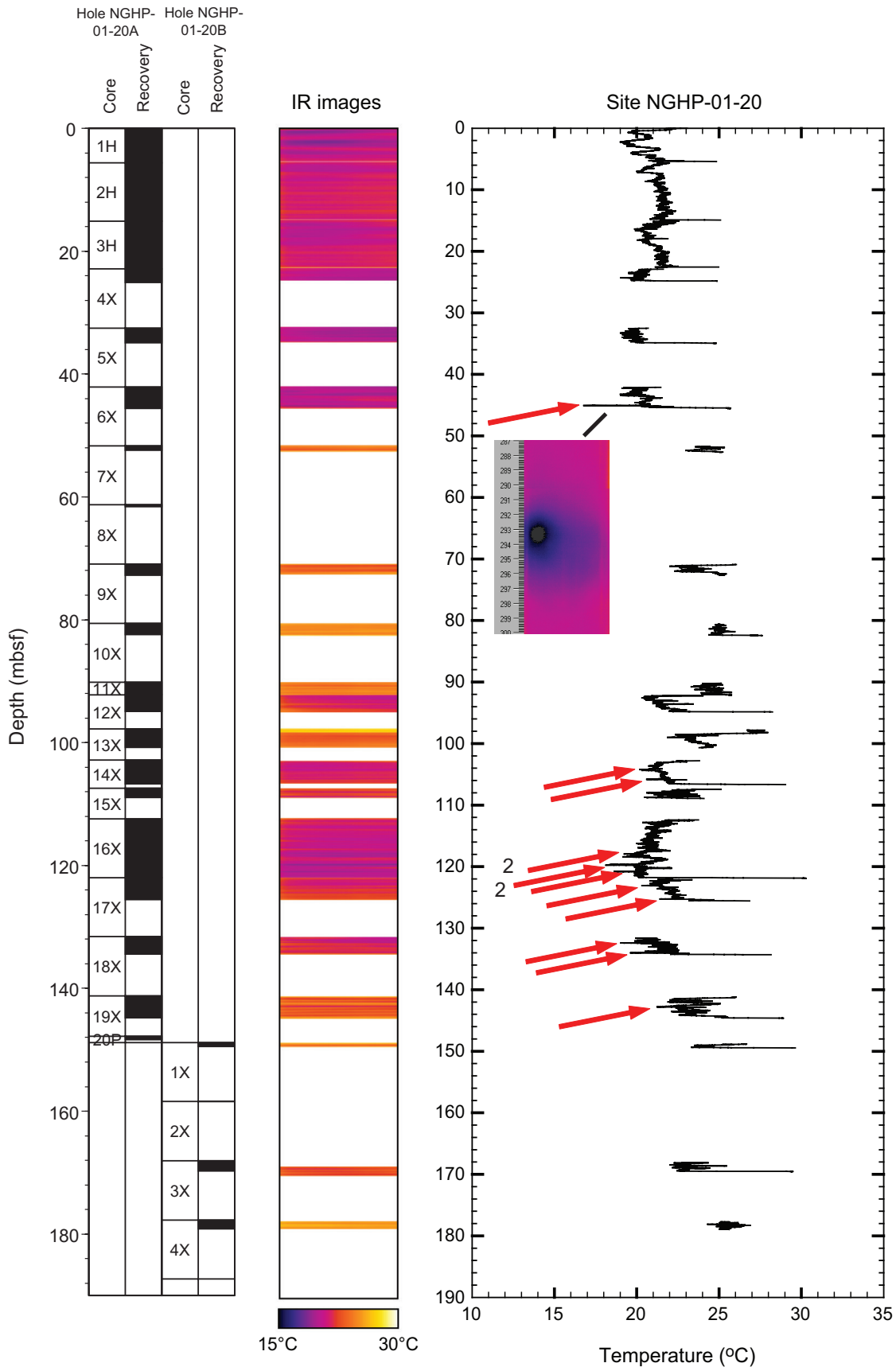
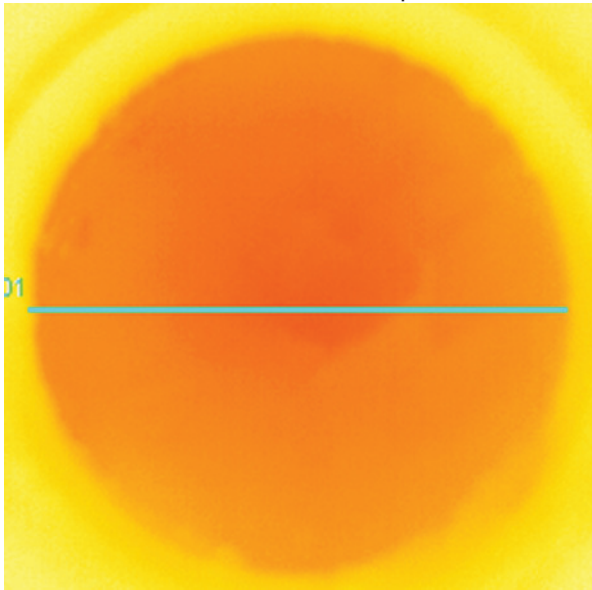


Figure 16. Infrared imaging and the derived downhole temperature profile for Site NGHP-01-20. Distinct cool zones in the core occur between ~104 and 144 mbsf and are shown by red arrows. [mbsf, meters below sea floor]

Section NGHP-01-20A-10X-2, Top



Section NGHP-01-20A-16X-3, Bottom

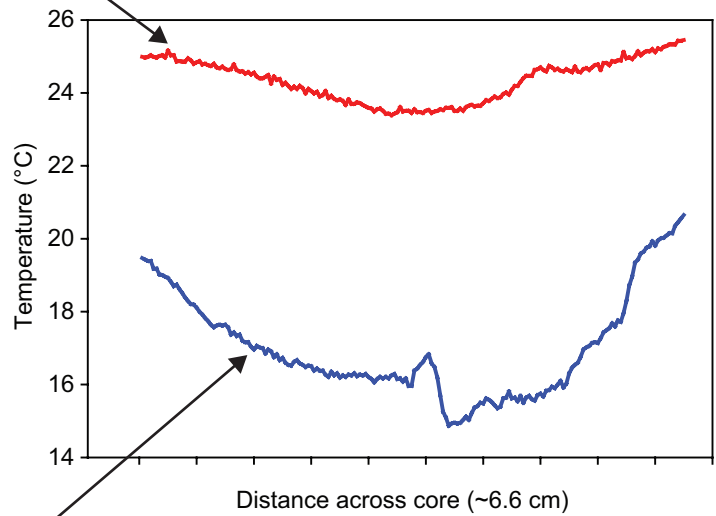
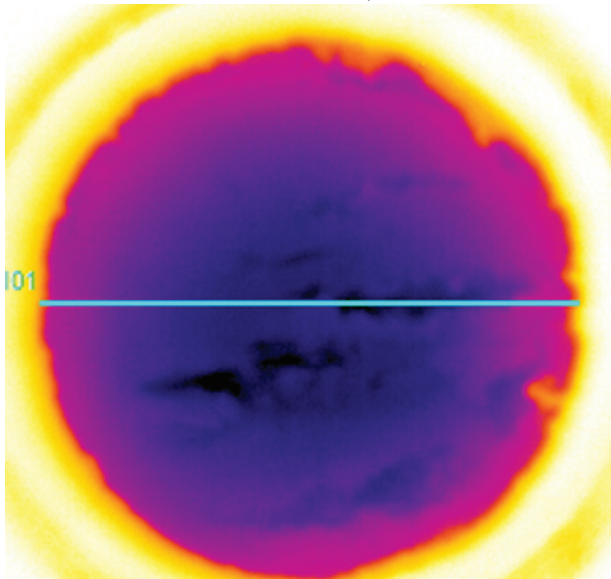


Figure 17. Comparison of core-end infrared images and cross-core temperature profiles from two different parts of Hole NGHP-01-20A: Cores NGHP-01-20A-10X and NGHP-01-20A-16X.

A rapid temperature drop occurred during the time of collection and scanning of the first four cores. No IR anomalies occur in these cores, so the interpretation of the IR anomalies is not affected. The cooler ambient temperatures during this time period do contribute slightly (<1 °C) to the apparent cooler temperatures of these shallow cores.

Core-End-Temperature Readings

Core-end-temperature readings were obtained on most cores immediately following the IR track imaging (table 10). Typically four temperature probes were inserted ~8 cm into the end of each core and allowed to remain there until the core was completely processed and removed from the catwalk. Temperatures from the center position probes were typically 5 to 10 °C less than the IR temperatures, as expected, since the IR images measure the liner temperature which has warmed closer to ambient temperatures than the center of the core, except where significant gas hydrate is present.

Index Properties

Although the measurement of physical properties (table 11 and figs. 18 and 19) was hampered by overall poor core recovery, the top of Hole NGHP-01-20A was adequately characterized because of good recovery in the first three APC cores. The upper 10 m of sediment has a typical reduction in water content and porosity and a corresponding increase in bulk density. Water content and porosity ranged from 140

percent (related to solids) and 78 percent respectively in the uppermost part of the core (table 11 and fig. 18) to 42 percent and 53 percent at the bottom of Hole NGHP-01-20B. A sandy layer at 24.7 mbsf has a water content of 22 percent and a porosity of 37 percent, the lowest values for this site.

Grain density varies from 2.55 to 2.76 g/cm³ at Site NGHP-01-20 (with an average value of 2.69 g/cm³) and is uniform below about 10 m (table 11 and fig. 18). However, from the seafloor to 10 mbsf, the grain density increases significantly from 2.55 to above 2.70 g/cm³. These low grain density values were encountered previously in the KG Basin during NGHP Expedition 01. At Site NGHP-01-20, three closely-spaced water content samples were obtained at numerous sub-bottom depths to check for the effect of sample size on grain density. Two of the samples were combined to increase the dry mass of the samples used in the pycnometers to obtain grain density. Overall, sample size had little effect on the measured grain density. Perhaps a higher organic content in the sediment near the seafloor is responsible for the lower grain densities.

Strength

Shear strength increases to 20 mbsf and then is varied to the bottom of the holes (tables 12 and 13, and fig. 18). Although the boundary between APC and XCB coring is about 23 mbsf, the erratic nature of the strength measurements begins above that depth indicating that it is not just the transition from push to rotary coring that is responsible for the difference in strengths.

Table 10. List of temperature probe data collected at bottom of cores from Hole NGHP-01-20A.

Core	Section	Bottom	Date	In time	Out time	Temperature probe #	Comments
1H	last	X	8/10				No probes, too short
1Ha	last	X	8/10	20:06	20:16	F-1, F-2, F-3, F-4	Pull away near tips of probes
2H	last	X	8/10	21:17	21:31	F-1, F-2, F-3, F-4	Perfect insert
3H	last	X	8/10	22:32	22:43	F-1, F-2, F-3, F-4	
4X	last	X	8/11	0:26	0:35	F-1, F-2, F-3, F-4	
5X	last	X	8/11	1:17	1:26	F-1, F-2, F-3, F-4	
6X	last	X	8/11	2:07	2:16	F-1, F-2, F-3, F-4	
7X			8/11				No probes
8X			8/11				No probes
9X	last	X	8/11	6:37	7:24	F-1, F-2, F-3, F-4	
10X	last		8/11	7:25	7:30	F-1, F-2, F-3, F-4	Small core diameter
11X			8/11				No probes (small core diameter)
12X			8/11				No probes ("sloppy" end)
13X	last	X	8/11	10:02	10:18	F-1, F-2, F-3, F-4	
14X	last	X	8/11	13:27	13:35	F-1, F-2, F-3, F-4	F-2 and F-3 only partially inserted, too hard, sticky
15X			8/11				No probes, broken up core
16X	last	X	8/11	15:40	15:54	F-1, F-2, F-3, F-4	Hard too pull out, but good insertion
17X	last	X	8/11	16:50	16:55	F-1, F-2, F-3, F-4	Good insertion on F-2 and F-3 (two middle probes)
18X	last	X	8/11	17:58	NA	F-1, F-2, F-3, F-4	
19X	last	X	8/11	18:53	NA	F-1, F-2, F-3, F-4	Poor insertion, not in all the way
1X							No probes
2X							No probes
3X	last	X	8/12	10:47	11:52	F-1, F-2, F-3, F-4	Hard sediment, probes not in all the way
4X	last	X	8/12	11:50	11:54	F-1, F-2, F-3, F-4	

Table 11. Moisture and density physical properties for Hole NGHP-01-20A.

Core, section	Sample	Depth, int, from (cm)	Depth, int, to (cm)	Depth (mbsf)	WCt (%)	WCs (%)	Grain density (g/cm ₃)	Bulk density (g/cm ₃)	Dry bulk density (g/cm ₃)	Porosity (%)	Void ratio	Unit weight (kN/m ³)
NGHP-01-20A												
1H-1	MAD	88	90	0.88	58.35	140.10	2.64	1.38	0.57	78.26	3.60	13.50
1H-1	MAD	88	90	0.88	52.43	110.22	2.63	1.45	0.69	74.25	2.88	14.25
1H-1	MAD	92	94	0.92	57.85	137.24	2.58	1.37	0.58	77.50	3.44	13.48
1H-2	MAD	62	64	2.12	54.97	122.07	2.55	1.40	0.63	75.20	3.03	13.77
1H-2	MAD	62	64	2.12	55.59	125.17	2.55	1.40	0.62	75.67	3.11	13.70
1H-3	MAD	50	52	3.50	46.79	87.94	2.61	1.52	0.81	69.08	2.23	14.86
1H-3	MAD	50	52	3.50	45.37	83.04	2.61	1.53	0.84	67.83	2.11	15.05
1H-3	MAD	53	55	3.53	44.70	80.82	2.61	1.54	0.85	67.24	2.05	15.14
1H-4	MAD	16	18	4.66	45.26	82.69	2.62	1.54	0.84	67.83	2.11	15.08
1H-4	MAD	16	18	4.66	45.71	84.18	2.62	1.53	0.83	68.22	2.15	15.02
1H-4	MAD	19	21	4.69	44.87	81.39	2.64	1.55	0.85	67.67	2.09	15.18
2H-1	MAD	101	103	6.61	46.77	87.86	2.62	1.52	0.81	69.16	2.24	14.88
2H-1	MAD	101	103	6.61	47.63	90.95	2.62	1.51	0.79	69.90	2.32	14.77
2H-1	MAD	104	106	6.64	47.18	89.32	2.63	1.52	0.80	70.08	2.34	14.95
2H-2	MAD	57	59	7.67	50.56	102.26	2.56	1.46	0.72	71.85	2.55	14.30
2H-2	MAD	57	59	7.67	49.96	99.83	2.56	1.47	0.73	71.36	2.49	14.37
2H-2	MAD	60	62	7.70	48.78	95.25	2.55	1.48	0.76	70.31	2.37	14.50
2H-3	MAD	90	92	9.50	39.58	65.51	2.61	1.62	0.98	62.53	1.67	15.88
2H-3	MAD	90	92	9.50	39.26	64.62	2.61	1.62	0.99	62.20	1.65	15.93
2H-3	MAD	94	96	9.54	38.15	61.69	2.68	1.66	1.03	61.72	1.61	16.26
2H-4	MAD	77	79	10.87	36.41	57.27	2.71	1.70	1.08	60.20	1.51	16.62
2H-4	MAD	77	79	10.87	36.42	57.27	2.71	1.69	1.08	60.21	1.51	16.62
2H-4	MAD	80	82	10.90	36.65	57.86	2.66	1.68	1.06	60.04	1.50	16.47
2H-5	MAD	44	46	12.04	36.51	57.50	2.65	1.68	1.07	59.82	1.49	16.47
2H-5	MAD	44	46	12.04	36.73	58.05	2.65	1.68	1.06	60.04	1.50	16.44
2H-5	MAD	47	49	12.07	30.53	43.94	2.66	1.79	1.24	53.23	1.14	17.53
2H-6	MAD	20	22	13.30	31.00	44.93	2.70	1.79	1.24	54.17	1.18	17.57
2H-6	MAD	20	22	13.30	31.95	46.96	2.70	1.77	1.21	55.26	1.24	17.39
2H-6	MAD	23	25	13.33	31.72	46.46	2.72	1.78	1.22	55.21	1.23	17.50
2H-6	MAD	67	69	13.77	30.37	43.61	2.71	1.81	1.26	53.51	1.15	17.72
2H-7	MAD	50	52	14.60	32.08	47.23	2.72	1.78	1.21	55.59	1.25	17.42
2H-7	MAD	50	52	14.60	32.16	47.40	2.72	1.78	1.20	55.68	1.26	17.41
2H-7	MAD	53	55	14.63	33.14	49.57	2.75	1.77	1.18	57.07	1.33	17.31
3H-1	MAD	58	60	15.68	35.73	55.59	2.65	1.69	1.09	59.01	1.44	16.59
3H-1	MAD	100	102	16.10	36.03	56.33	2.67	1.70	1.09	59.76	1.49	16.66
3H-2	MAD	7	9	16.67	34.58	52.87	2.72	1.73	1.13	58.35	1.40	16.95
3H-2	MAD	81	83	17.41	36.38	57.19	2.71	1.69	1.08	60.17	1.51	16.61
3H-3	MAD	19	21	18.29	35.39	54.79	2.72	1.72	1.11	59.28	1.46	16.82
3H-3	MAD	102	104	19.12	33.29	49.91	2.74	1.76	1.17	57.18	1.34	17.25
3H-4	MAD	11	13	19.71	32.69	48.56	2.74	1.77	1.19	56.51	1.30	17.37
3H-4	MAD	72	74	20.32	31.50	45.98	2.75	1.79	1.23	55.16	1.23	17.59
3H-5	MAD	16	18	21.26	42.13	72.81	2.76	1.61	0.93	66.22	1.96	15.79
3H-5	MAD	96	98	22.06	31.87	46.78	2.74	1.79	1.22	55.53	1.25	17.51
4X-1	MAD	42	44	23.32	37.20	59.24	2.72	1.68	1.06	61.14	1.57	16.51
4X-2	MAD	17	19	24.57	33.16	49.61	2.73	1.76	1.18	56.97	1.32	17.26

Table 11. Moisture and density physical properties for Hole NGHP-01-20A.—Continued

Core, section	Sample	Depth, int, from (cm)	Depth, int, to (cm)	Depth (mbsf)	WCt (%)	WCs (%)	Grain density (g/cm ₃)	Bulk density (g/cm ₃)	Dry bulk density (g/cm ₃)	Porosity (%)	Void ratio	Unit weight (kN/m ³)
NGHP-01-20A—Continued												
4X-2	MAD	30	32	24.70	18.36	22.50	2.70	2.08	1.69	37.21	0.59	20.36
5X-1	MAD	31	33	32.81	33.65	50.72	2.74	1.75	1.16	57.57	1.36	17.17
5X-2	MAD	29	31	34.29	33.94	51.39	2.71	1.74	1.15	57.67	1.36	17.06
6X-1	MAD	32	34	42.42	34.62	52.96	2.70	1.72	1.13	58.29	1.40	16.90
6X-2	MAD	25	27	43.85	23.49	30.69	2.69	1.94	1.49	44.60	0.81	19.06
6X-2	MAD	73	75	44.33	32.33	47.77	2.70	1.77	1.20	55.79	1.26	17.32
6X-3	MAD	14	16	44.74	31.07	45.08	2.73	1.80	1.24	54.60	1.20	17.64
6X-4	MAD	11	13	45.27	33.67	50.77	2.74	1.75	1.16	57.59	1.36	17.17
7X-1	MAD	40	42	52.10	31.91	46.86	2.69	1.77	1.21	55.23	1.23	17.36
9X-1	MAD	37	39	71.27	31.43	45.83	2.71	1.78	1.22	54.81	1.21	17.50
9X-2	MAD	13	15	72.53	31.75	46.52	2.72	1.78	1.22	55.32	1.24	17.48
10X-1	MAD	26	28	80.86	34.95	53.72	2.71	1.72	1.12	58.71	1.42	16.85
10X-2	MAD	13	15	82.23	31.67	46.34	2.67	1.77	1.21	54.70	1.21	17.33
11X-1	MAD	28	30	90.48	29.19	41.22	2.71	1.83	1.30	52.19	1.09	17.93
11X-2	MAD	13	15	91.83	27.21	37.38	2.69	1.86	1.36	49.60	0.98	18.29
12X-1	MAD	64	66	92.84	27.50	37.93	2.73	1.87	1.36	50.27	1.01	18.33
12X-2	MAD	93	95	94.63	25.36	33.97	2.72	1.92	1.43	47.51	0.90	18.79
13X-1	MAD	91	93	98.71	28.90	40.65	2.69	1.83	1.30	51.64	1.07	17.92
13X-2	MAD	60	62	99.62	31.05	45.04	2.71	1.79	1.24	54.43	1.19	17.58
13X-3	MAD	35	37	100.62	32.10	47.27	2.75	1.78	1.21	55.93	1.27	17.48
14X-1	MAD	40	42	103.20	28.97	40.80	2.72	1.84	1.31	52.08	1.09	18.03
14X-2	MAD	45	47	104.75	33.42	50.21	2.71	1.75	1.16	57.10	1.33	17.14
15X-1	MAD	28	30	107.68	31.49	45.96	2.74	1.79	1.23	55.20	1.23	17.58
16X-1	MAD	22	24	112.62	34.23	52.04	2.72	1.74	1.14	58.07	1.38	17.02
16X-2	MAD	22	24	114.12	32.44	48.02	2.73	1.77	1.20	56.14	1.28	17.36
16X-3	MAD	46	48	115.86	32.12	47.32	2.72	1.78	1.21	55.75	1.26	17.41
16X-4	MAD	52	54	117.42	34.38	52.39	2.71	1.73	1.13	58.11	1.39	16.96
16X-5	MAD	52	54	118.92	33.58	50.56	2.72	1.75	1.16	57.31	1.34	17.12
16X-6	MAD	15	17	119.55	35.59	55.25	2.71	1.71	1.10	59.41	1.46	16.75
16X-7	MAD	44	46	120.35	34.82	53.43	2.75	1.73	1.13	58.95	1.44	16.98
16X-8	MAD	37	39	121.13	28.97	40.79	2.73	1.84	1.31	52.11	1.09	18.04
17X-2	MAD	22	24	123.32	30.38	43.63	2.73	1.81	1.26	53.83	1.17	17.78
17X-3	MAD	26	28	124.86	34.04	51.60	2.71	1.73	1.14	57.72	1.37	17.01
18X-1	MAD	35	37	131.95	34.32	52.26	2.75	1.74	1.14	58.42	1.41	17.07
18X-2	MAD	35	37	132.95	33.06	49.39	2.74	1.76	1.18	56.99	1.32	17.29
18X-3	MAD	27	29	133.87	33.18	49.66	2.74	1.76	1.18	57.07	1.33	17.25
19X-1	MAD	35	37	141.55	34.74	53.23	2.71	1.72	1.13	58.55	1.41	16.91
19X-2	MAD	23	25	142.93	31.35	45.67	2.73	1.79	1.23	54.97	1.22	17.59
19X-3	MAD	25	27	144.45	29.25	41.34	2.74	1.84	1.30	52.59	1.11	18.04
20P-1	MAD	42	44	148.22	31.88	46.80	2.72	1.78	1.21	55.45	1.24	17.45
NGHP-01-20B												
1X-1	MAD	29	31	149.09	39.76	65.99	2.72	1.64	0.99	63.70	1.75	16.07
3X-1	MAD	38	40	168.48	33.29	49.90	2.72	1.75	1.17	57.04	1.33	17.19
3X-1	MAD	64	66	168.74	30.39	43.65	2.72	1.81	1.26	53.73	1.16	17.74
4X-1	MAD	8	10	177.78	29.65	42.14	2.75	1.83	1.29	53.08	1.13	17.96

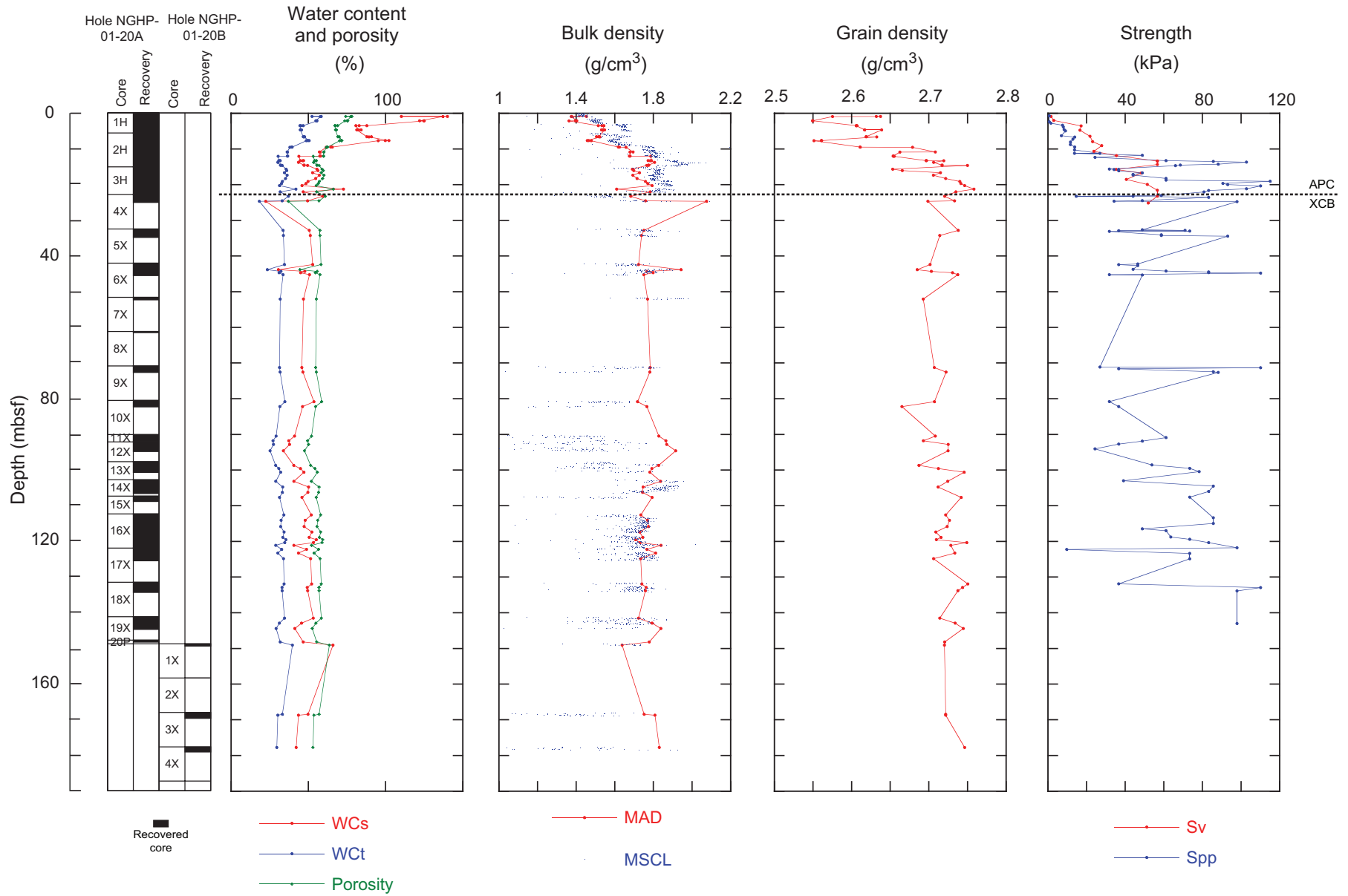


Figure 18. Profiles of core recovery, index, and strength properties for Site NGHP-01-20. [MAD, moisture and density physical properties; MSCL, MultiSensor Core Logger]

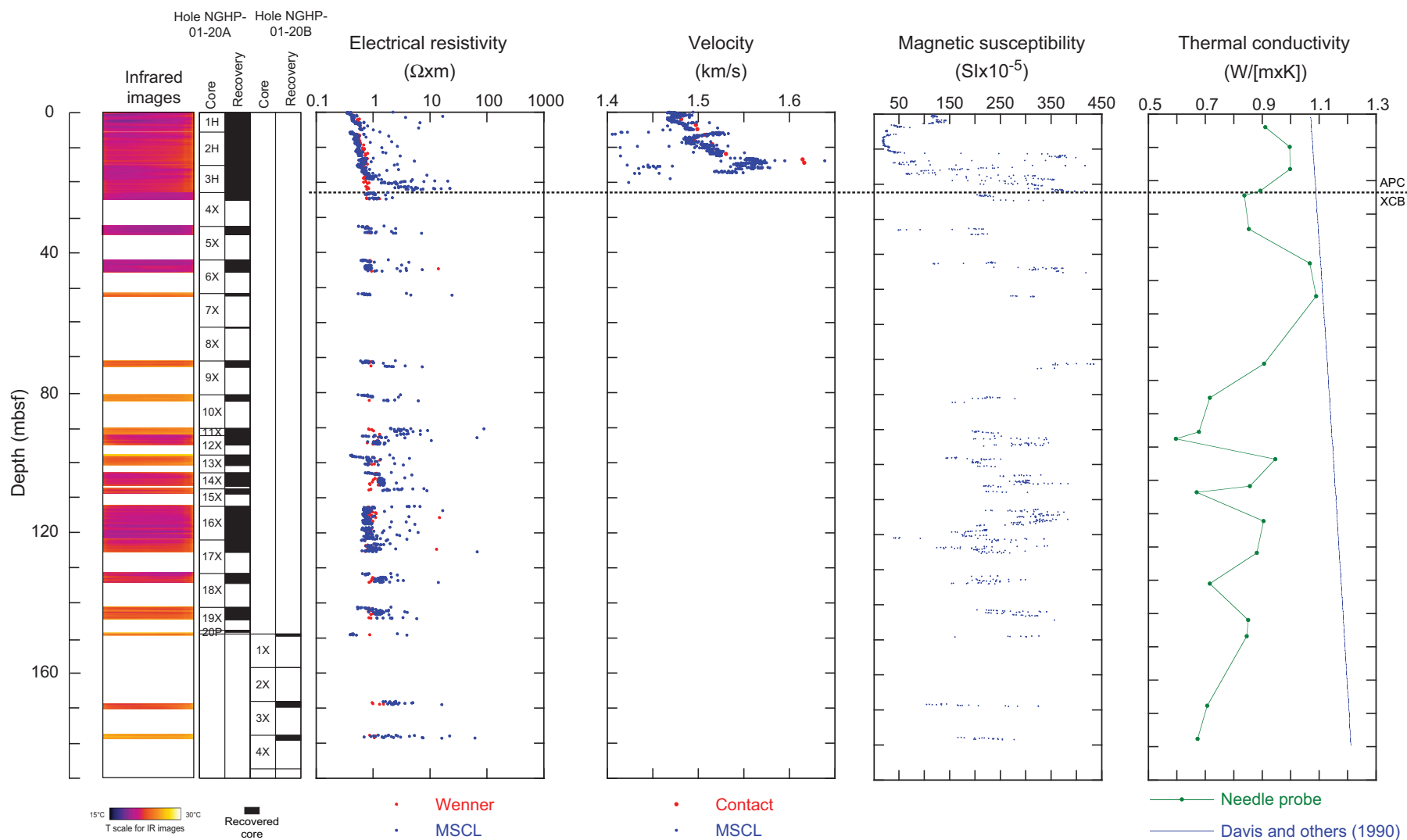


Figure 19. Profiles of infrared images, core recovery, electrical resistivity, acoustic *P*-wave velocity, magnetic susceptibility, and thermal conductivity for Site NGHP-01-20.

Table 12. Vane shear strength results for Hole NGHP-01-20A.

Core, section	Sample	Top (cm)	Depth (mbsf)	Sv (kPa)	Sres (kPa)	Srem (kPa)	St
NGHP-01-20A							
1H-1	VS	91	0.91	1.6	1.2	0.8	2.0
1H-2	VS	49	1.99	3.1	2.0	1.3	2.4
1H-3	VS	55	3.55	17.2	13.2	4.4	3.9
1H-4	VS	25	4.75	16.7	9.9	4.9	3.4
2H-1	VS	86	6.46	21.9	13.2	7.2	3.0
2H-2	VS	84	7.94	23.2	13.2	6.7	3.4
2H-3	VS	45	9.05	28.0	18.1	8.6	3.3
2H-4	VS	55	10.65	23.9	13.6	9.9	2.4
2H-5	VS	27	11.87	35.5	23.0	12.9	2.8
3H-1	VS	65	15.75	35.4	23.0	13.2	2.7
3H-2	VS	17	16.77	48.4	31.3	19.9	2.4
4H-2	VS	77	18.57	40.6	22.2	14.8	2.7
3H-3	VS	47	19.96	51.5	31.3	21.4	2.4
4X-1	VS	33	25.17	52.0	28.0	6.8	7.6

The measured shear strengths were normalized to the effective vertical stress (σ'_v) (fig. 20) to provide qualitative information on the stress history of the sediment. The strength/effective vertical stress ratio ranges from ~1.4 at the top to an average of about 0.1 deeper in the hole. The values between the seafloor and 35 mbsf are substantially greater than 0.4 and indicate that the sediment is overconsolidated. Below that level, the values are in overall agreement with a number of other normally consolidated clays (Holtz and Kovacs, 1981). Hunt (1984) states that the strength/effective vertical stress ratio typically is between 0.4 and 0.16. The wide scatter in the results at the top of the hole reflects the dependency of this ratio on the stress path as well as the test method (Bjerrum, 1972; Ladd and others, 1977). Because the values are typically greater than 0.4 above 35 m, the implication is that these sediments have experienced a vertical effective stress greater than what is now being applied *in situ*. They have been overconsolidated by erosional or other geologic processes.

The peak (Sv) and remolded (Srem) vane shear strengths clearly increase with subbottom depth (fig. 21). The sensitivity (St), which equals Sv/Srem, typically varies between 2 and 4, with one point at 7.6. Sensitivity values represent the amount of strength loss after remolding—in extreme examples they can reach values of 500 (Lambe and Whitman, 1969). This sediment has low to medium sensitivity (Holtz and Kovacs, 1981). High values of sensitivity are indicative of good quality core recovery because the sediment has not been highly disturbed.

Electrical Resistivity

Strong agreement exists between electrical resistivity values produced by the MSCL and the contact Wenner array (fig. 19). The resistivity values determined using the Wenner array on split cores typically are on the low side of the MSCL data (fig. 19), in part because the Wenner measurements are conducted on intact core material, rather than a wider portion of core that may contain voids, small expansion cracks, or

slurry. Lower MSCL values are more representative of undisturbed sediment as they are less impacted by the presence of micro voids caused by gas expansion.

Resistivity determined using the MSCL (fig. 19) increases at 18 mbsf which is very close to the depth of the SMI at 17 mbsf. A possible explanation for this agreement is that methane is produced below the SMI and this gas expands upon core recovery disrupting the sediment structure. However, the Wenner values at this site do not reflect an increased resistivity at the SMI.

The apparent formation factor is the ratio of the resistivity of a saturated sediment to the resistivity of the pore fluid. This ratio provides an indication of the relationships between sediment structure, void space, tortuosity, and other factors, and the ability of fluid to flow through the formation. Because pore water salinity typically varies a small amount in the recovered sediment and is similar to that of seawater (see “Inorganic Geochemistry”), we have normalized the measured Wenner resistivity values by using that of seawater (~0.2 Ω -m) (table 14). Values range from about 2.5 at the top of the hole to typically less than 6.0 at the bottom, although a few points as high as 8.0 are present (fig. 22). Other equations and methods exist for calculating the formation factor; however, they require the use of empirical constants that have not yet been determined for the sediments at this location.

P-Wave Velocity

P-wave velocity (V_p) measured with the MSCL increased slightly from 1.46 km/s in the top of the hole (fig. 19) to 1.57 km/s at a subbottom depth of 18 m, which represents the depth where gas and voids present in the sediment prevented further valid measurements from being logged. The contact V_p values of 1.48 to 1.62 km/s (table 15) are in overall agreement with the MSCL data. However, the V_p 's measured at the two deepest locations are higher than the MSCL values and are the fastest contact V_p values recorded during NGHP Expedition 01. These high velocities are again confirmation of the overconsolidated nature of the sediment. Valid contact V_p measurements could not be determined below 16 mbsf. Both techniques are adversely affected by the SMI located at about 17 mbsf (see “Organic Geochemistry” and “Inorganic Geochemistry”). Methane, which is typically produced below the SMI, may come out of solution if present in a high enough concentration and attenuate acoustic signals.

Magnetic Susceptibility

Magnetic susceptibility values are quite high and variable below about 11 mbsf (fig. 19). These values are in agreement with the magnetic susceptibility values found in holes drilled previously in the KG Basin during Expedition NGHP-01 and are due to the presence of primary and secondary terrigenous magnetic minerals (see “Lithostratigraphy”).

Table 13. Pocket Penetrometer strength results for Hole NGHP-01-20A.

Core, section	Sample	Top (cm)	Depth (mbsf)	Spp (kPa)	Core, section	Sample	Top (cm)	Depth (mbsf)	Spp (kPa)
NGHP-01-20A					NGHP-01-20A—Continued				
1H-1	PP	77	0.77	0.8	5X-1	PP	63	33.13	31.9
1H-2	PP	90	2.40	0.8	5X-2	PP	8	34.08	58.8
1H-2	PP	126	2.76	1.5	5X-2	PP	26	34.26	58.8
1H-3	PP	35	3.35	7.7	5X-2	PP	46	34.46	93.1
1H-3	PP	87	3.87	8.0	6X-1	PP	18	42.28	46.6
1H-4	PP	10	4.60	8.4	6X-1	PP	38	42.48	36.8
1H-4	PP	48	4.98	9.2	6X-1	PP	60	42.70	46.6
2H-1	PP	72	6.32	7.0	6X-2	PP	17	43.77	44.1
2H-1	PP	112	6.72	13.9	6X-2	PP	64	44.24	61.3
2H-2	PP	20	7.30	13.0	6X-2	PP	91	44.51	83.3
2H-2	PP	100	8.10	11.8	6X-3	PP	8	44.68	83.3
2H-3	PP	20	8.80	11.6	6X-3	PP	24	44.84	110.3
2H-3	PP	84	9.44	13.9	6X-4	PP	8	45.24	31.9
2H-4	PP	20	10.30	13.8	6X-4	PP	20	45.36	49.0
2H-4	PP	113	11.23	27.0	9X-1	PP	27	71.17	27.0
2H-4	PP	117	11.27	13.8	9X-1	PP	46	71.36	110.3
2H-5	PP	20	11.80	49.0	9X-1	PP	74	71.64	36.8
2H-5	PP	78	12.38	24.5	9X-2	PP	5	72.45	85.8
2H-6	PP	16	13.26	61.3	9X-2	PP	23	72.63	88.2
2H-6	PP	44	13.54	85.8	10X-1	PP	20	80.80	31.9
2H-6	PP	60	13.70	102.9	10X-2	PP	15	82.25	36.8
2H-7	PP	21	14.31	88.2	11X-1	PP	73	90.93	61.3
2H-7	PP	44	14.54	68.6	11X-2	PP	18	91.88	49.0
2H-7	PP	60	14.70	66.2	12X-1	PP	55	92.75	36.8
3H-1	PP	56	15.66	31.9	12X-2	PP	40	94.10	24.5
3H-1	PP	63	15.73	36.8	13X-1	PP	79	98.59	53.9
3H-1	PP	69	15.79	34.3	13X-2	PP	52	99.54	73.5
3H-1	PP	104	16.14	36.8	13X-3	PP	19	100.46	78.4
3H-2	PP	13	16.73	49.0	14X-1	PP	23	103.03	39.2
3H-2	PP	54	17.14	44.1	14X-2	PP	23	104.53	85.8
3H-2	PP	75	17.35	44.1	14X-3	PP	23	106.03	83.3
3H-3	PP	17	18.27	61.3	15X-1	PP	23	107.63	73.5
3H-3	PP	63	18.73	61.3	16X-1	PP	100	113.40	85.8
3H-3	PP	98	19.08	115.2	16X-2	PP	110	115.00	85.8
3H-4	PP	9	19.69	90.7	16X-3	PP	110	116.50	49.0
3H-4	PP	43	20.03	93.1	16X-4	PP	10	117.00	61.3
3H-4	PP	80	20.40	110.3	16X-5	PP	40	118.80	63.7
3H-5	PP	8	21.18	102.9	16X-6	PP	4	119.44	73.5
3H-5	PP	54	21.64	83.3	16X-7	PP	42	120.33	83.3
3H-5	PP	100	22.10	80.9	16X-8	PP	102	121.78	98.0
4X-1	PP	16	23.06	58.8	17X-1	PP	29	122.29	9.8
4X-1	PP	39	23.29	14.7	17X-2	PP	30	123.40	73.5
4X-1	PP	40	23.30	44.1	17X-3	PP	31	124.91	73.5
4X-1	PP	69	23.59	83.3	18X-1	PP	30	131.90	36.8
4X-2	PP	9	24.49	49.0	18X-2	PP	36	132.96	110.3
4X-2	PP	23	24.63	34.3	18X-3	PP	31	133.91	98.0
4X-2	PP	39	24.79	98.0	19X-2	PP	34	143.04	98.0
5X-1	PP	18	32.68	49.0	NGHP-01-20B				
5X-1	PP	34	32.84	71.1	3X-1	PP	40	168.50	85.8
5X-1	PP	42	32.92	36.8	3X-1	PP	62	168.72	110.3
5X-1	PP	52	33.02	73.5	4X-1	PP	64	178.34	85.8

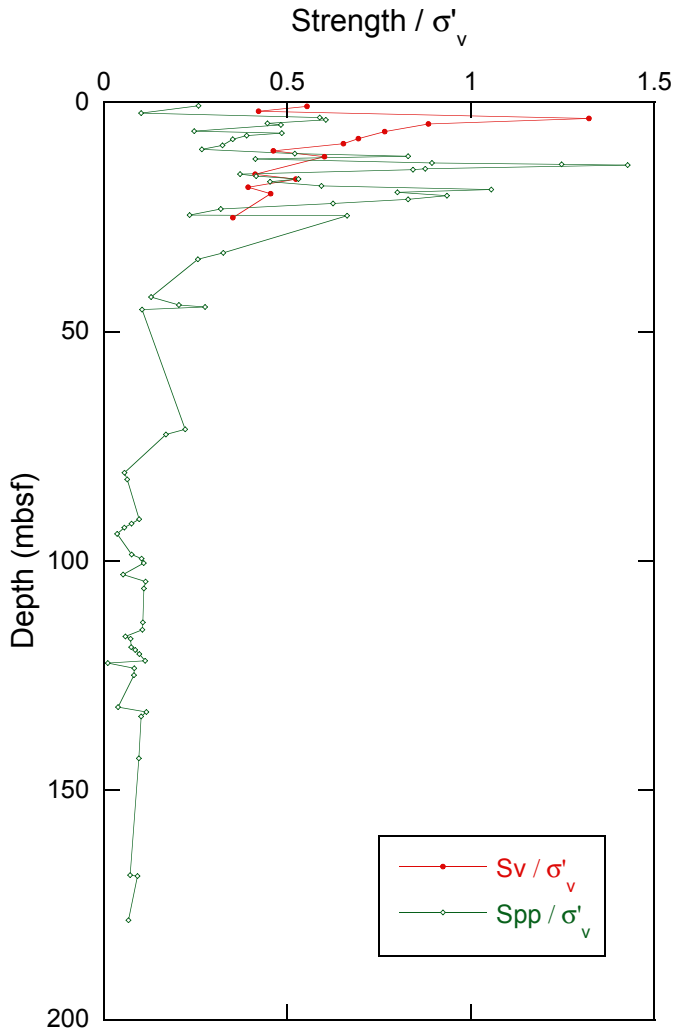


Figure 20. Shear strengths normalized to the effective vertical stress versus sub-bottom depth for Hole NGHP-01-20A.

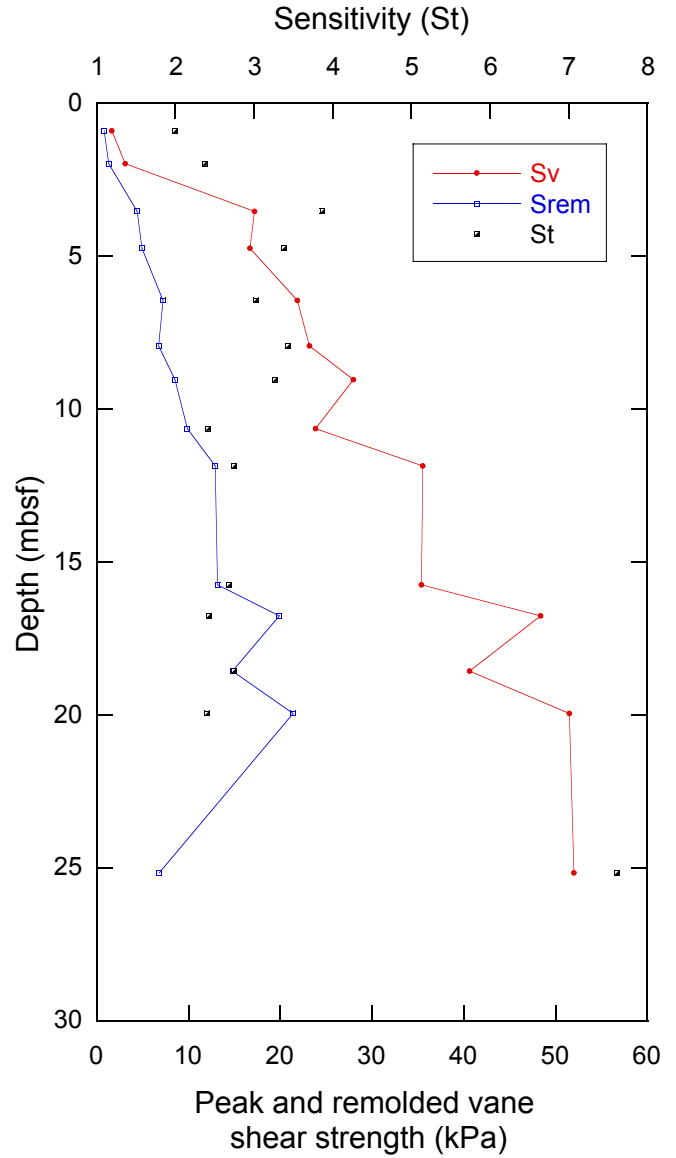


Figure 21. Peak and remolded vane shear strengths and sensitivity for Hole NGHP-01-20A. [Sv, peak vane shear strength; Srem, remolded vane shear strength; St, shear strength sensitivity]

Table 14. Wenner array electrical resistivity and formation factor results for Hole NGHP-01-20A.

Core, section	Sample	Top (cm)	Depth (mbsf)	Electrical resistivity (W×m)	Apparent formation factor	Core, section	Sample	Top (cm)	Depth (mbsf)	Electrical resistivity (W×m)	Apparent formation factor
NGHP-01-20A											
1H-1	ER	78	0.78	0.439	2.197	3H-2	ER	95	17.55	0.725	3.623
1H-2	ER	45	1.95	0.579	2.895	3H-3	ER	15	18.25	0.748	3.742
1H-2	ER	65	2.15	0.533	2.663	3H-3	ER	35	18.45	0.708	3.539
1H-2	ER	85	2.35	0.533	2.664	3H-3	ER	55	18.65	0.736	3.678
1H-2	ER	105	2.55	0.538	2.691	3H-3	ER	75	18.85	0.679	3.393
1H-2	ER	125	2.75	0.556	2.779	3H-3	ER	95	19.05	0.730	3.648
1H-3	ER	25	3.25	0.571	2.855	3H-4	ER	15	19.75	0.749	3.744
1H-3	ER	45	3.45	0.573	2.866	3H-4	ER	35	19.95	0.684	3.418
1H-3	ER	65	3.65	0.588	2.941	3H-4	ER	55	20.15	0.856	4.281
1H-4	ER	15	4.65	0.613	3.063	3H-4	ER	75	20.35	0.795	3.975
1H-4	ER	35	4.85	0.601	3.004	3H-5	ER	10	21.20	0.747	3.736
2H-1	ER	86	6.46	0.562	2.810	3H-5	ER	30	21.40	0.794	3.971
2H-1	ER	106	6.66	0.587	2.933	3H-5	ER	50	21.60	0.813	4.066
2H-2	ER	15	7.25	0.564	2.819	3H-5	ER	70	21.80	0.842	4.212
2H-2	ER	35	7.45	0.566	2.829	3H-5	ER	90	22.00	0.782	3.912
2H-2	ER	55	7.65	0.570	2.849	4X-1	ER	15	23.05	0.943	4.713
2H-2	ER	75	7.85	0.551	2.754	4X-1	ER	35	23.25	0.782	3.912
2H-2	ER	95	8.05	0.560	2.802	4X-1	ER	58	23.48	0.778	3.889
2H-2	ER	115	8.25	0.588	2.938	4X-2	ER	7	24.47	0.768	3.841
2H-3	ER	15	8.75	0.592	2.960	4X-2	ER	25	24.65	0.773	3.866
2H-3	ER	35	8.95	0.600	3.001	4X-2	ER	30	24.70	1.307	6.537
2H-3	ER	55	9.15	0.610	3.052	4X-2	ER	37	24.77	0.862	4.310
2H-3	ER	75	9.35	0.684	3.420	5X-1	ER	20	32.70	0.803	4.015
2H-4	ER	15	10.25	0.651	3.257	5X-1	ER	36	32.86	0.768	3.840
2H-4	ER	35	10.45	0.711	3.553	5X-1	ER	54	33.04	0.809	4.044
2H-4	ER	55	10.65	0.695	3.474	5X-2	ER	19	34.19	0.918	4.591
2H-4	ER	75	10.85	0.663	3.315	5X-2	ER	43	34.43	0.857	4.286
2H-4	ER	95	11.05	0.601	3.004	6X-1	ER	20	42.30	0.879	4.395
2H-4	ER	115	11.25	0.668	3.338	6X-1	ER	40	42.50	0.918	4.592
2H-5	ER	15	11.75	0.803	4.016	6X-1	ER	63	42.73	0.866	4.331
2H-5	ER	35	11.95	0.734	3.672	6X-2	ER	16	43.76	0.825	4.126
2H-5	ER	55	12.15	0.742	3.710	6X-2	ER	37	43.97	0.849	4.243
2H-5	ER	75	12.35	0.728	3.638	6X-2	ER	67	44.27	0.756	3.781
2H-6	ER	15	13.25	0.799	3.996	6X-2	ER	89	44.49	0.799	3.993
2H-6	ER	35	13.45	0.765	3.827	6X-3	ER	18	44.78	0.781	3.903
2H-6	ER	54	13.64	0.721	3.603	6X-4	ER	20	45.36	0.940	4.699
2H-7	ER	15	14.25	0.748	3.742	7X-1	ER	40	52.10	0.797	3.983
2H-7	ER	35	14.45	0.735	3.675	9X-1	ER	36	71.26	0.906	4.531
2H-7	ER	55	14.65	0.624	3.119	9X-1	ER	59	71.49	0.865	4.326
2H-7	ER	75	14.85	0.796	3.982	9X-2	ER	2	72.42	0.918	4.590
3H-1	ER	55	15.65	0.718	3.588	10X-1	ER	25	80.85	0.795	3.975
3H-1	ER	75	15.85	0.687	3.433	10X-2	ER	15	82.25	0.858	4.289
3H-1	ER	95	16.05	0.738	3.692	11X-1	ER	19	90.39	0.839	4.194
3H-1	ER	115	16.25	0.714	3.571	11X-1	ER	35	90.55	0.858	4.290
3H-2	ER	10	16.70	0.730	3.652	11X-1	ER	39	90.59	0.954	4.768
3H-2	ER	30	16.90	0.754	3.768	11X-1	ER	75	90.95	1.024	5.119
3H-2	ER	50	17.10	0.719	3.593	11X-2	ER	20	91.90	1.310	6.548
3H-2	ER	70	17.30	0.695	3.476	12X-1	ER	58	92.78	1.241	6.206
3H-2	ER	72	17.32	0.726	3.632	12X-2	ER	11	93.81	1.242	6.211
3H-2	ER	76	17.36	0.782	3.910	12X-2	ER	30	94.00	1.032	5.159
3H-2	ER	85	17.45	0.739	3.696	12X-2	ER	60	94.30	0.791	3.955
3H-2	ER	90	17.50	0.703	3.517	12X-2	ER	99	94.69	1.002	5.009

Table 14. Wenner array electrical resistivity and formation factor results for Hole NGHP-01-20A.—Continued

Core, section	Sample	Top (cm)	Depth (mbsf)	Electrical resistivity (W×m)	Apparent formation factor	Core, section	Sample	Top (cm)	Depth (mbsf)	Electrical resistivity (W×m)	Apparent formation factor
NGHP-01-20A—Continued						NGHP-01-20A—Continued					
13X-1	ER	74	98.54	1.041	5.204	16X-5	ER	73	119.13	0.806	4.029
13X-1	ER	85	98.65	0.822	4.108	16X-5	ER	88	119.28	0.845	4.227
13X-2	ER	22	99.24	1.321	6.606	16X-6	ER	12	119.52	0.743	3.715
13X-2	ER	38	99.40	0.911	4.554	16X-7	ER	27	120.18	0.827	4.136
13X-2	ER	55	99.57	0.916	4.581	16X-7	ER	53	120.44	0.953	4.763
13X-3	ER	11	100.38	1.056	5.280	16X-8	ER	22	120.98	0.785	3.927
13X-3	ER	24	100.51	0.956	4.780	16X-8	ER	42	121.18	0.931	4.654
14X-1	ER	10	102.90	0.861	4.305	16X-8	ER	91	121.67	0.786	3.928
14X-1	ER	25	103.05	1.165	5.824	17X-1	ER	12	122.12	0.701	3.506
14X-1	ER	39	103.19	1.049	5.243	17X-2	ER	20	123.30	1.120	5.600
14X-1	ER	52	103.32	1.056	5.280	17X-2	ER	40	123.50	0.807	4.035
14X-2	ER	20	104.50	1.089	5.444	17X-2	ER	60	123.70	0.740	3.700
14X-2	ER	40	104.70	1.212	6.061	17X-2	ER	80	123.90	0.859	4.297
14X-2	ER	60	104.90	1.012	5.060	17X-2	ER	101	124.11	1.015	5.076
14X-2	ER	80	105.10	1.217	6.086	17X-2	ER	121	124.31	0.921	4.606
14X-2	ER	100	105.30	1.502	7.509	17X-2	ER	141	124.51	0.934	4.668
14X-2	ER	120	105.50	0.976	4.880	17X-3	ER	18	124.78	0.790	3.949
14X-3	ER	25	106.05	0.873	4.365	17X-3	ER	38	124.98	0.948	4.738
14X-3	ER	42	106.22	0.893	4.464	17X-3	ER	56	125.16	0.849	4.244
14X-3	ER	57	106.37	1.236	6.182	17X-3	ER	73	125.33	0.734	3.668
15X-1	ER	20	107.60	0.916	4.581	18X-1	ER	20	131.80	0.742	3.709
15X-1	ER	40	107.80	0.849	4.243	18X-2	ER	20	132.80	0.985	4.926
16X-1	ER	24	112.64	0.815	4.073	18X-2	ER	44	133.04	1.048	5.239
16X-1	ER	41	112.81	0.838	4.191	18X-2	ER	65	133.25	0.954	4.769
16X-1	ER	60	113.00	0.832	4.160	18X-2	ER	79	133.39	0.962	4.808
16X-1	ER	80	113.20	0.917	4.587	18X-3	ER	19	133.79	0.919	4.594
16X-1	ER	100	113.40	0.949	4.746	18X-3	ER	36	133.96	1.340	6.698
16X-1	ER	113	113.53	0.896	4.481	18X-3	ER	54	134.14	0.853	4.264
16X-2	ER	20	114.10	0.902	4.511	19X-1	ER	35	141.55	0.865	4.326
16X-2	ER	20	114.10	0.996	4.982	19X-1	ER	55	141.75	0.843	4.215
16X-2	ER	40	114.30	1.117	5.587	19X-1	ER	75	141.95	0.847	4.236
16X-2	ER	60	114.50	1.140	5.700	19X-1	ER	95	142.15	0.915	4.577
16X-2	ER	80	114.70	0.861	4.307	19X-1	ER	125	142.45	0.829	4.145
16X-2	ER	100	114.90	0.877	4.385	19X-2	ER	17	142.87	1.157	5.785
16X-2	ER	105	114.95	0.909	4.545	19X-2	ER	41	143.11	0.982	4.910
16X-2	ER	120	115.10	0.953	4.763	19X-2	ER	58	143.28	0.915	4.576
16X-3	ER	24	115.64	1.120	5.599	19X-3	ER	7	144.27	0.850	4.251
16X-3	ER	40	115.80	0.857	4.284	19X-3	ER	17	144.37	0.914	4.568
16X-3	ER	64	116.04	0.913	4.564	NGHP-01-20B					
16X-3	ER	80	116.20	0.878	4.392	1X-1	ER	29	149.09	0.876	4.380
16X-3	ER	105	116.45	0.776	3.879	3X-1	ER	40	168.50	0.966	4.830
16X-3	ER	120	116.60	0.866	4.328	3X-1	ER	62	168.72	0.995	4.975
16X-3	ER	130	116.70	0.997	4.983	3X-1	ER	79	168.89	1.528	7.640
16X-4	ER	20	117.10	0.833	4.167	3X-1	ER	81	168.91	1.309	6.545
16X-4	ER	43	117.33	0.898	4.489	4X-1	ER	9	177.79	0.879	4.395
16X-5	ER	17	118.57	0.846	4.231	4X-1	ER	28	177.98	1.112	5.560
16X-5	ER	37	118.77	0.837	4.185	4X-1	ER	74	178.44	1.049	5.245
16X-5	ER	57	118.97	0.936	4.682						

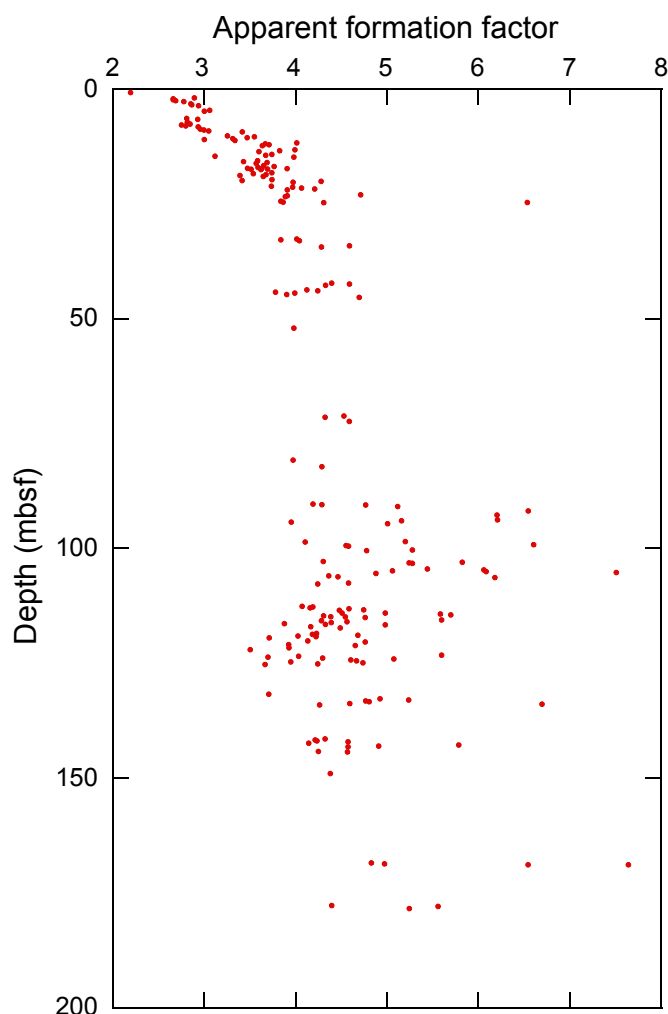


Figure 22. Apparent formation factor versus sub-bottom depth for Hole NGHP-01-20A.

Thermal Conductivity

Thermal conductivities vary between 0.597 and 1.091 W/(m×K) and decrease somewhat with subbottom depth (table 16 and fig. 19). Such values are well within the range of marine sediments, although they are all lower than values determined by Davis and others (1990) for sediment from Cascadia and the Nankai Trough.

Downhole Temperature Measurements

A number of different tools are available for determining downhole sediment temperature (see “Physical Properties” section of “Methods” chapter). At Site NGHP-01-20, only two attempts were made to measure *in situ* temperature (table 17 and fig. 23). Both provided very good quality data. The apparent thermal gradient indicated by these two measurements is 49 °C per km with a seafloor intercept of 5.5 °C (shipboard calculated seafloor temperature 4.8 °C, geothermal gradient 50 °C per km).

Pressure Coring

No pressure cores were recovered at Site NGHP-01-20. The single pressure core recovery attempted, Core NGHP-01-20A-20P, was unsuccessful, and no further pressure core recoveries were attempted due to poor hole conditions.

Downhole Logging

No wireline logging was performed at Site NGHP-01-20 due to poor hole conditions.

Table 15. Contact *P*-Wave velocity results determined on split cores sections from Hole NGHP-01-20A.

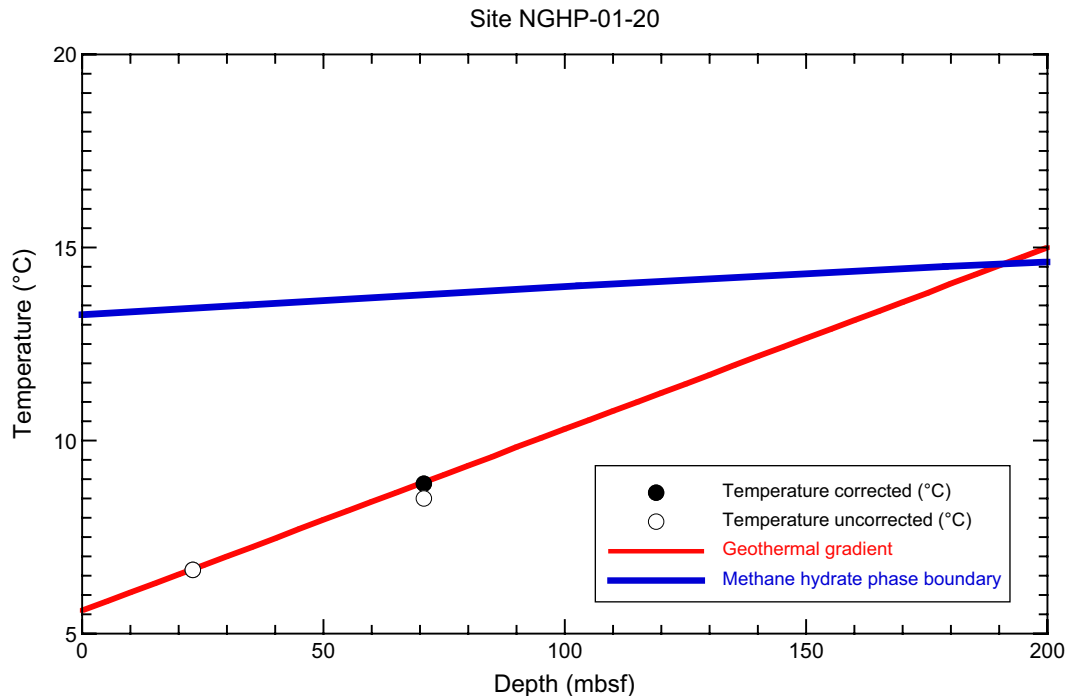
Core, section	Sample	Top (cm)	Depth (mbsf)	VP (m/s)	VP (km/s)
NGHP-01-20A					
1H-1	VP	91	0.91	1481.24	1.481
1H-2	VP	50	2	1481.24	1.481
1H-3	VP	65	3.65	1497.29	1.497
1H-4	VP	36	4.86	1498.92	1.499
2H-1	VP	85	6.45	1507.09	1.507
2H-2	VP	75	7.85	1495.67	1.496
2H-3	VP	55	9.15	1515.35	1.515
2H-4	VP	55	10.65	1520.35	1.520
2H-5	VP	35	11.95	1530.45	1.530
2H-6	VP	36	13.46	1614.49	1.614
2H-7	VP	36	14.46	1616.37	1.616

Table 16. Thermal conductivity results for Hole NGHP-01-20A.

Core, section	Sample	Top (cm)	Depth (mbsf)	Thermal conductivity (W/(m×K))
NGHP-01-20A				
1H-3	TC	75	3.75	0.911
2H-3	TC	75	9.35	0.997
3H-1	TC	60	15.70	0.998
3H-5	TC	80	21.90	0.894
4X-1	TC	35	23.25	0.838
5X-1	TC	35	32.85	0.853
6X-1	TC	50	42.60	1.067
7X-1	TC	27	51.97	1.091
9X-1	TC	35	71.25	0.907
10X-1	TC	35	80.95	0.716
11X-1	TC	50	90.70	0.678
12X-1	TC	50	92.70	0.597
13X-1	TC	70	98.50	0.946
14X-3	TC	40	106.20	0.857
15X-1	TC	52	107.92	0.670
16X-3	TC	75	116.15	0.905
17X-3	TC	60	125.20	0.881
18X-3	TC	40	134.00	0.716
19X-3	TC	17	144.37	0.851
NGHP-01-20B				
1X-1	TC	21	149.01	0.846
3X-1	TC	75	168.85	0.707
4X-1	TC	59	178.29	0.673

Table 17. *In situ* temperature estimates for Hole NGHP-01-20A.

Depth (mbsf)*	Core	Thermal conductivity (W/[m×K])	Tool	Temperature (°C)	Ad hoc calibration correction	Corrected temperature (°C)	Estimated uncertainty	Data quality
22.9	A03H	0.95	APCT-3	6.65	0.00	6.65	0.1	good
70.9	A09X	0.95	DVTP	8.5	0.50	8.89	0.2	good

**Figure 23.** Geothermal gradient and estimated depth to the BSR from *in situ* temperature measurements for Hole NGHP-01-20A. [BSR, bottom-simulating reflector]

References Cited

- Bjerrum, L., 1972, Embankments on soft ground, *in* ASCE Specialty Conference on Performance of Earth and Earth-Supported Structures, Lafayette, Ind., June 11–14, 1972, Proceedings: New York, American Society of Civil Engineers, v. 2, p. 1–54. [Held at Purdue University]
- Davis, E.E., Hyndman, R.D., and Villinger, H., 1990, Rates of fluid expulsion across the northern Cascadia accretionary prism—Constraints from new heat flow and multichannel seismic reflection data: *Journal of Geophysical Research*, v. 95, p. 8869–8889.
- Duan, Z., Møller, N., Greenberg, J., and Weare, J.H., 1992, The prediction of methane solubility in natural waters to high ionic strengths from 0° to 250 °C and from 0 to 1600 bar: *Geochim Cosmochim Acta*, no. 56, p. 1451–1460.
- Holtz, R.D. and Kovacs, W.D., 1981, *An introduction to geotechnical engineering*: Englewood Cliffs, N. J., Prentice-Hall, Inc., 733 p.
- Hunt, R.E., 1984, *Geotechnical engineering investigation manual*: New York, McGraw-Hill Book Company, 983 p.
- Ladd, C.C., Foote, R., Ishihara, K., Schlosser, F., and Poulos, H.G., 1977, Stress-deformation and strength characteristics, *in* State-of-the-Art Report, Ninth International Conference on Soil Mechanics and Foundation Engineering, Tokyo, Japan, July 10–15, 1977., v. 2, p. 421–494.
- Lambe, T. William, Whitman, Robert V., 1969, *Soil mechanics*: New York, John Wiley and Sons, 553 p.
- Musgrave, R.J., Bangs, N.L., Larrasoana, J.C., Gracia, E., Hollamby, J.A., Vega, M.E., 2006, Rise of the base of the gas hydrate zone since the last glacial recorded by rock magnetism: *Geology*, v. 34, no. 2, p. 117–120.
- Xu, W., 2002, Phase balance and dynamic equilibrium during formation and dissociation of methane gas hydrate, *in* 4th International Conference on Gas Hydrates, Yokohama, Japan, May 19–23, 2002, Proceedings: 4th International Conference on Gas Hydrates, Yokohama, Japan, p. 195–200.
- Xu, W., 2004, Modeling dynamic marine gas hydrate systems: *American Mineralogist*, v. 89, p. 1271–1279.